Detailed analysis of particulate emissions of a multi-cylinder dual-mode dual-fuel engine operating with diesel and gasoline

Fuel 330 (2022) 125578

https://doi.org/10.1016/j.fuel.2022.125578

Antonio García, Javier Monsalve-Serrano*, David Villalta and Álvaro Fogué-Robles

CMT - Motores Térmicos, Universitat Politècnica de València, Camino de Vera s/n, 46022 Valencia, Spain

Corresponding author (*):

Dr. Javier Monsalve-Serrano (jamonse1@mot.upv.es)

Phone: +34 963876559

Fax: +34 963876559

Abstract

Internal combustion engines are still within the future of highway transport. Low-temperature combustion modes are prone to substitute conventional diesel combustion engines, seeking better performance and improved emissions control. The dual-mode dual-fuel combustion approach has been confirmed as a feasible combustion mode for achieving ultra-low NOx and soot emissions simultaneously. The aim of this work is to experimentally measure the particle emissions of the dual-mode dual-fuel concept while maintaining good thermal efficiency and EURO VI engine-out NOx levels. A detailed analysis of the most relevant characteristics of the particle size distribution is carried out to depict the requirements of a potential filtering system considering the effects of an upstream diesel oxidation catalyst. The results show that total particle numbering is within the typical values of the current most popular technologies: around $2 \cdot 10^{13}$ #/kWh for RCCI and around 10^{14} #/kWh for DMDF. RCCI combustion tends to produce more particles sized below 35 nm in diameter, while DMDF shows a clear dominance of sizes above 40 nm. In terms of total particulate matter, RCCI results in total mass concentrations around 4 mg/kWh thanks to the highly premixed combustion, but diffusive combustion mode results in total mass emissions over 50 mg/kWh.

Keywords

Reactivity controlled compression ignition; after treatment system; Particle Numbering; Particulate Matter; EURO VI

1. Introduction

In recent years, growing concern about air pollution and global warming has resulted in dramatic judgments on emissions limits across the board. This has impacted the transportation sector in particular, as it is estimated that it is responsible for around 21% of the global CO_2 emissions. However, the most stringent measures are being applied to the road transport sector for two main reasons: it has the highest share of total emissions in the transport sector (around 15% of global emissions) and is the one closest to the population, thus posing the most significant risk to people's health [1].

The permissible limits of various pollutants particular to internal combustion engines (ICEs) have undergone a substantial drop in recent years, among the many limitations put on fuel-based vehicles. As evidence, in the previous ten years, changes to the permissible limits have resulted in reductions of more than 75 percent in nitrogen oxides (NOx) emissions in Europe and China and more than 90 percent in the United States. Due to the high conversion efficiency of modern after-treatment systems (ATS), the limit for partially oxidized hydrocarbons (HC) has been reduced by roughly 65 percent, but the limit for carbon monoxide (CO) has remained relatively unchanged. Finally, particulate matter emissions have been limited to less than half of what they were previously [2]. To meet these goals, the present ATS is significantly more complex and costly to incorporate specialized devices to remove the individual species targeted.

The constringent effect of these limitations has made other technologies rise as potential substitutes for current conventional engines based on fossil fuels. Battery electric vehicles have become a competitor for light-duty applications, with clear benefits for decarbonization of vehicles [3], but their application for heavy-duty applications still suffers critical drawbacks in terms of autonomy and payload capacity [4]. Alternative fuels with no carbon content like hydrogen are also a rising star conceptualized explicitly for the transport sector, but this new technology implies other concerns regarding logistics and infrastructure, so research and development time prior to its final product application is still needed [5]. For these reasons, the development of more efficient combustion strategies for conventional engines is necessary as a temporal solution during the transition to other new alternatives [6,7].

With what is known as low-temperature combustion (LTC) modes, several writers in the literature have investigated the prospect of bringing together a solution for both difficulties, lowering controlled species emissions while increasing engine efficiency. This approach of decreasing combustion temperatures helps to significantly minimize NOx and soot generation while also reducing heat losses and increasing the engine's overall efficiency. Early fuel injections are used in most of the concepts in the literature to promote a more homogeneous fuel-to-air mixture while controlling combustion phasing and peak temperatures with high rates of exhaust gas recirculation (EGR), but a more conceptual definition of the strategy is required to ensure a certain level of performance. The homogeneous charge compression ignition (HCCI), partially premixed combustion (PPC), premixed charge compression ignition (PCCI), gasoline compression ignition (GCI), and reactivity-controlled compression ignition (RCCI) are among the most successful LTC concepts developed in the last decade for compression ignition (CI) engines [8].

All these approaches have proven effective in reporting ultra-low levels of NOx and soot emissions while maintaining or improving fuel efficiency when compared to conventional diesel engines. The use of strongly premixed combustion has the disadvantage of not being suited for high engine loads, which is one of the fundamental limits of traditional LTC modes, which cannot cover the whole operating range of the map. Benajes et al. [9] employed dual-fuel RCCI combustion with a high reactivity fuel (HRF) and a low reactivity fuel (LRF) as a starting point and adjusted the combustion strategy to get more stratified mixtures at medium engine loads and more diffusive diesel-like combustion at full engine load. The reactivity of the mixture is controlled by a near-homogeneous load of an LRF introduced through the port fuel injectors (PFI) and a stratified charge of HRF introduced through the direct injector (DI) in an LTC concept called dual-mode dual-fuel (DMDF). It uses a more homogeneous-like or partly stratified injection technique at low and medium loads and a more diesel-like diffusive combustion strategy at greater loads, where it performs better and delivers higher power rates [10]. The DMDF combustion concept has been tested and assessed, and the findings reveal that utilizing gasoline as the LRF and diesel as the HRF can achieve EURO VI engine-out NOx and soot levels. In this method, the SCR in charge of NOx reduction [11] can be removed from the ATS, lowering manufacturing costs and lowering the effect of its installation [12] as well as concerns about ammonia slip [11].

One of the critics of the RCCI combustion concept is that, despite showing ultra-low particulate matter (PM) emissions verified by smoke numbering and opacity, this does not mean that no particles are being emitted since depending on the principle of the measuring device [13] the correlation of conventional particle matter devices is no longer valid for ultra-low particle emissions of low-temperature advance combustion modes [14]. The treatment of particle number (PN) and PM on the EURO regulation has varied significantly over time, and its latest version includes a limit for both parameters.

Therefore the need to consider not only total mass but also the number of particles emitted [15,16]. Some authors have shown that RCCI combustion can produce relatively high particle emissions in terms of particle PN compared to fully premixed combustion modes like HCCI [17]. Nonetheless, dedicated studies to evaluate the DMDF combustion mode while targeting NOx and soot levels below EU VI limits are scarce. Bermudez et al. [18] investigated the effect of injection settings on particle emissions in a dual-fuel single-cylinder engine, and Benajes et al. [19] showed the impact of reaching ultra-low NOx over the particle size distribution in a single-cylinder engine. Additionally, the usage of alternative fuels in blends [20] or dual fuel systems [21] has demonstrated a huge potential to improve the performance of the engine [22] as well as emissions, reaching ultra-low particle emissions for certain fuels like polyoxymethylene dimethyl ethers [23].

The current paper aims to carry out a dedicated study on the particle size distribution (PSD) and particle numbering emitted by a medium-duty 7.7L multi-cylinder engine characteristic of heavy-duty transport applications modified to operate under DMDF combustion mode capable of maintaining EURO VI NOx levels and ultra-low smoke numbering when operating in RCCI mode, moving from single-cylinder studies to a complete system evaluation. Detailed analysis of the effect of the combustion mode over total PN and the characteristics of the PSD is produced. Considering the high concentration of condensates that can appear due to high emissions of HC and CO coming from the high levels of EGR and premixed ratios employed, the effect of a commercial DOC [24] is also accounted for so that the inlet conditions of a potential DPF can also be defined.

2. Materials and Methods

2.1. Engine characteristics

Experimental work was carried out on a 7.7L multi-cylinder production engine modified to include a new fuel supply circuit for 6 PFI required to inject LRF into the intake manifold and a low-pressure EGR circuit for increased control flexibility. A new piston with optimized geometry for better control over the combustion process and emissions with a reduced compression ratio from 17.5:1 to 12.75:1 ensures proper operation and stability at high loads. Particulate matter is present in the EGR that passes through the low-pressure EGR circuit, so a DPF must be installed to protect the turbocharger.

Table 1. Engine characteristics.

Engine Characteristics	
Engine Type	4 stroke, 4 valves, direct injection
Number of cylinders [-]	6
Displaced volume [cm^3]	7700
Stroke [mm]	135
Bore [mm]	110
Piston bowl geometry [-]	Bathtub
Compression ratio [-]	12.75:1
Rated power [kW]	235 @ 2100 rpm
Rated torque [Nm]	1200 @ 1050-1600 rpm

2.2. Test cell description

The engine is installed on an AVL active dynamometer for safe and proper operation, and the engine speed is controlled using its own software platform, AVL PUMA Open. The same platform is used to record averaged pressures and temperatures at various system locations, fresh air mass flow using an airflow meter at the intake, and average fuel consumption using two gravimetric fuel balances, one for LRF and the other for HRF.

Because of the system's complexity, which includes two EGR circuits and two injection systems, an external graphic interface was created in LabView to command the DI and PFI systems separately, as well as different control parameters such as injection pressure, valve positioning (EGR and back pressure valves), and VGT rack position. The LabView interface is coupled to an encoder with a precision of 0.2 crank angle degrees for reference injection time (CAD).

Readings and records of various instantaneous magnitudes, such as the chamber pressure of all six cylinders, as well as data from external equipment devoted to emissions measurements, are also stored on the external control platform. For the gaseous emissions measuring, the test cell counts with a five-gas Horiba MEXA-7100 DEGR analyzer [25] for NOx, CO, HC, O_2, and CO_2. An AVL 415 smoke meter [26] allows quantifying the smoke content as normally measured. Lastly, a dedicated setup for PSD characterization composed of a dilution system based on a rotating disc MD19-3E from Testo [27] that allows to freeze the particle distribution sample and protects the other devices from excessive particle concentration, and a Scanning Mobility Particle Sizer (SMPS) from TSI [28] to characterize the size distribution of the sample. The installation also includes a DOC in the exhaust line, so, in order to characterize the effect that this catalyst has on the particulate matter, a set of line selectors allow to change the measuring location of the Horiba gas analyzer and the SMPS so that engine-out emissions and after-DOC composition can be measured.

An in-cylinder thermodynamic analysis is done in two phases, using all of the observations of instantaneous and averaged magnitudes. The first is an online study based on apparent heat release that is applied in the LabView control system to enable a more detailed examination of combustion during engine operation. The second phase is a more in-depth thermodynamic study based on the recorded data. This post-processing is carried out with CMT's CALMEC software, which consists of a collection of pre-calibrated models for doing a complete 0D combustion study [29].

Figure 1 shows a thorough schematic distribution of all of the equipment in the test cell, and Table 2 lists the specific models and critical accuracies of the measurement instruments. This information has been used to carry out an uncertainty analysis following the procedure stated in the work from [30] to ensure that the reported values have accuracy and repetitiveness within acceptable values. This information has not been included in the manuscript for the brevity of the document, but all error values can be reproduced using the referenced methodology.

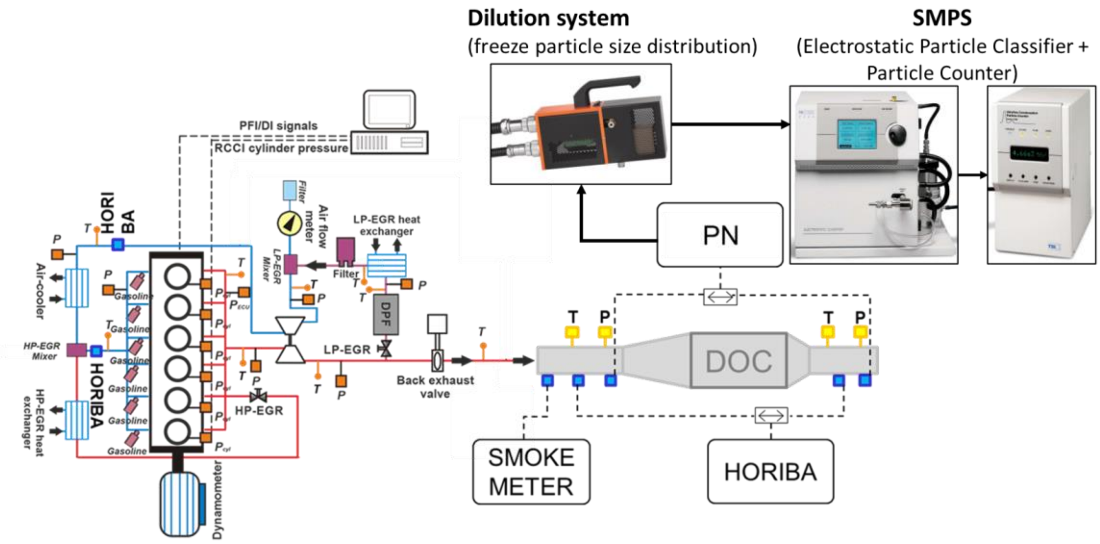

Figure 1. Test cell diagram.

Table 2. Accuracy of the instrumentation used in this work.

Variable measured	Device	Manufacturer / model	Accuracy
In-cylinder pressure	Piezoelectric transducer	Kistler / 6125C	±1.25 bar
Intake/exhaust pressure	Piezoresistive transducers	Kistler / 4045A	±25 mbar
Temperature in settling chambers and manifolds	Thermocouple	TC direct / type K	±2.5 °C
Crank angle, engine speed	Encoder	AVL / 364	±0.02 CAD
NOx, CO, HC, O_2, CO_2	Gas analyser	HORIBA / MEXA 7100 DEGR	4%
FSN	Smoke meter	AVL / 415	±0.025 FSN
PN	Particle Counter	TSI/SMPS 3936	±1 #/cm^3 (bin)
Gasoline/diesel fuel mass flow	Fuel balances	AVL / 733S	±0.2%
Air mass flow	Air flow meter	Elster / RVG G100	±0.1%

2.3. Fuels and injection systems characteristics

Diesel fuel is utilized as the HRF, and gasoline is used as the LRF in this study. Table 3 summarizes the basic physicochemical features of these fuels.

Table 3. Physical and chemical properties of gasoline and the different high reactivity fuels evaluated.

	EN 590 diesel	EN 228 gasoline
Density [kg/m^3] (15 °C)	842	720
Viscosity [mm^2/s] (40 °C)	2.93	0.545
Cetane number [-]	55.7	-
Carbon content [% m/m]	86.2	84.4
Hydrogen content [% m/m]	13.8	15.6
Oxygen content [% m/m]	0	0
RON [-]	-	95.6
MON [-]	-	85.7
Lower heating value [MJ/kg]	42.44	42.4
Vapor pressure [hPa] (T=40 °C)	1-10	450-650

During the intake phase, the dual-fuel concept allows controlling the in-cylinder charge creation and stratification by injecting the LRF through the PFI placed at each cylinder intake pipe to establish a homogenous base air-to-fuel mixture and then injecting the HRF through the DI system during the compression stroke. It is feasible to achieve the required load reactivity distribution by adjusting the amount of each fuel, the HRF start of injection (SOI), and the common rail injection pressure to have some control over the mixing rate. The features of both injector types are presented in Table 4 for a simple characterization of both injection systems.

Table 4. Characteristics of the different injectors.

DI Injector		PFI Injector	
Actuation Type [-]	Solenoid	Injector Style [-]	Saturated
Steady flow rate @ 100 bar [cm^3/min]	1300	Steady flow rate @ 3 bar [cm^3/min]	980
Included spray angle [°]	150	Included Spray Angle [°]	30
Number of holes [-]	7	Injection Strategy [-]	single
Hole diameter [µm]	177	Start of Injection [CAD ATDC]	340
Maximum injection pressure [bar]	2500	Maximum injection pressure [bar]	5.5

2.4. Methodology for experimental evaluation

A systematic calibration technique is used on a total of 36 operation conditions spread over the engine's whole range of operation. The engine speed ranged from 950 to 2200 rpm, and the load increase was divided into 10%, 25%, 50%, 60%, 75%, and 100% relative to the highest nominal power production at each engine speed as depicted in Figure 2b.

The combustion mode employed along the engine map is the DMDF concept devised at CMT [31], in which dual-fuel RCCI transitions towards dual-fuel diffusive combustion as the engine load increases, according to the conceptual sketch shown in Figure 2a. The engine settings employed in this study are based on an EU VI calibration that targets NOx and soot emissions from FSN readings that were previously produced. The primary target to maintain NOx emissions under EURO VI was ensured via online measurement of NOx emissions and different mass flows, pressures, and temperatures during the tests, which were then used to correct the specific NOx emissions considering ambient humidity in accordance with the standard procedure dictated by the EURO norm. The final specific emissions had to be below 0.4 g/kWh to accept them as fulfilling the stationary limit of EURO VI. The limits for avoiding mechanical issues in the engine were the same as for the EU VI calibration (in-cylinder P_{max} 180 bar, PRR 17.5 bar/CAD). More details about the injection settings and other aspects of the calibration can be consulted in the work from Sari R. et al. [31].

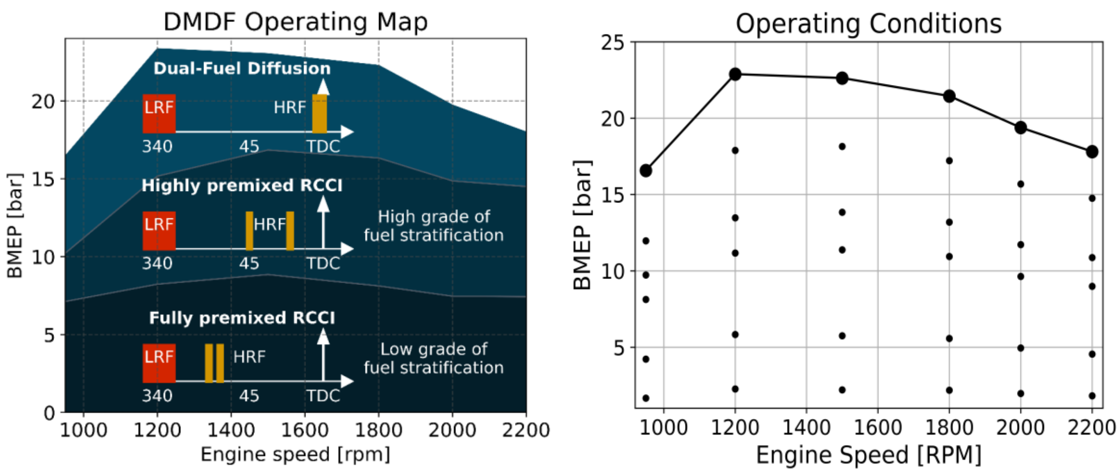

(a) (b)

Figure 2. Conceptual injection strategy of the dual-mode dual-fuel combustion concept (a) and operating conditions included in this evaluation (b).

Measuring conditions and gas thermodynamic state can highly affect the total particle number measured since the mechanisms of nucleation, accumulation, and aggregation that are part of the formation path of solid particles can be accelerated or halted depending on temperature, concentration, and other thermodynamic and compositional parameters [32]. According to classical nucleation theory [33,34], the processes of forming new particles through nucleation and evaporation of existing nuclei show a certain hysteresis, as represented in the phase diagram of Figure 3. This allows freezing the particle sample as long as the sample is extracted following a rapid path that allows it to go from point A to point D avoiding the formation or evaporation of particles during the measuring time. The rotating disk dilution technique allows following a path that resembles that defined by A-C-D.

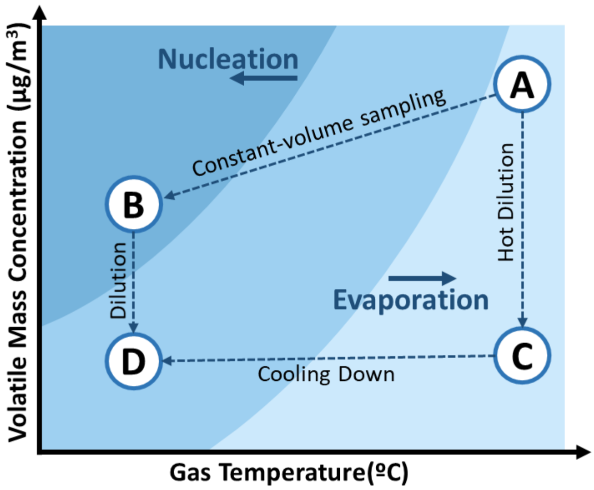

Figure 3. Conceptual phase diagram of volatile substances (adapted from [27]).

The efficacy of this technique is defined mainly by the temperature of the diluting gas, the dilution ratio, and the sampling rate. In the literature, several rules of thumb can be found to define these parameters. In this study, the methodology developed by Fuentes E. [35] and later corroborated by Soto L. [36] on the same equipment model employed in this study has been applied to fix the settings of the SMPS and find the appropriate dilution ratio necessary at each operating condition to ensure a static sample and a safe operation of the measuring equipment. The final setup allows measuring particles in the range of 5-240 nm to focus on the fine particles in the exhaust line that usually are harder to treat by the ATS and always provide a particle concentration lower than 10^8 particles/cm^3 not to saturate the sample above the maximum limit of the device [28].

During the post-processing, the final PSD is computed by correcting the reported measurement of particle concentration with the dilution ratio [37].

3. Results and discussion

This section includes different subsections covering the study of particulate emissions and how the DOC affects the distribution of particle number and total particulate mass in order to evaluate the performance of the RCCI and DMDF combustion modes compared to other technologies as well as provide some guidelines and boundary conditions to define which are the requirements of an appropriate DPF. In addition to this information, other measurements that might be relevant for the comprehension of the results are included in the Appendix, including engine performance parameters, other relevant pollutants, and boundary conditions of the DOC. These results have been previously reported in other publications, but in order for the manuscript to be self-contained, these parameters have been properly referenced and briefly explained in the Appendix.

3.1. Engine out emissions

The most direct indicator of the particles emitted by the engine is the total amount of particles or the PN, which for heavy-duty applications is reported as a specific emission in terms of #/kWh. Figure 4 shows the total PN throughout all the engine map covered by the 36 points measured for this analysis, following the requirements for EURO VI regulation, in which only particles above 23 nm are considered. The reported values show emissions levels that vary from 10^{12} to $4\cdot10^{14}$ #/kWh depending on the region of the map. These values clearly surpass the $8\cdot10^{11}$ #/kWh limit imposed by the current regulation, evidencing the need for dedicated analysis of this specific emission and how to control it.

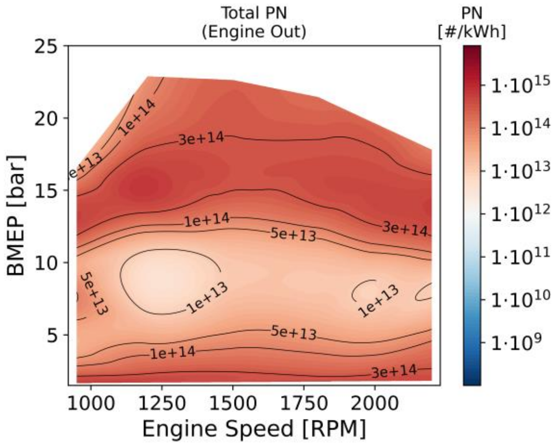

Figure 4. Engine out Particle Number emissions of the DMDF combustion mode.

The tendencies observed on the map also show how the total particles are affected as the engine load is increased, having a significant reduction at moderate loads. This can be related to two main parameters of the DMDF combustion mode: injection timing and gasoline fraction. Comparing the tendencies on PN emissions from Figure 4 with the combustion settings evolution represented in Figure 5, it can be concluded that both very early injections and high premixing rates allow for reducing particle formation. This combination provides a highly premixed load within the cylinder that permits the formation of excessively rich regions generally attributed to the formation of large particles as well as advancing the combustion, giving more time for oxidizing particles during the closed cycle of the cylinder.

Above 50% load, where premixing is no longer possible due to significant pressure gradients that reach the mechanical limit of the hardware, combustion mode is transitioned towards more diffusive combustion, lowering the utilization of LRF and delaying the injection timing of HRF, which is also accompanied with the formation of a load that is getting globally richer with the load. From these modifications, particle formation is significantly enhanced [38], and total emissions of particles reach their maximum values within the operating region of the map tested in this evaluation.

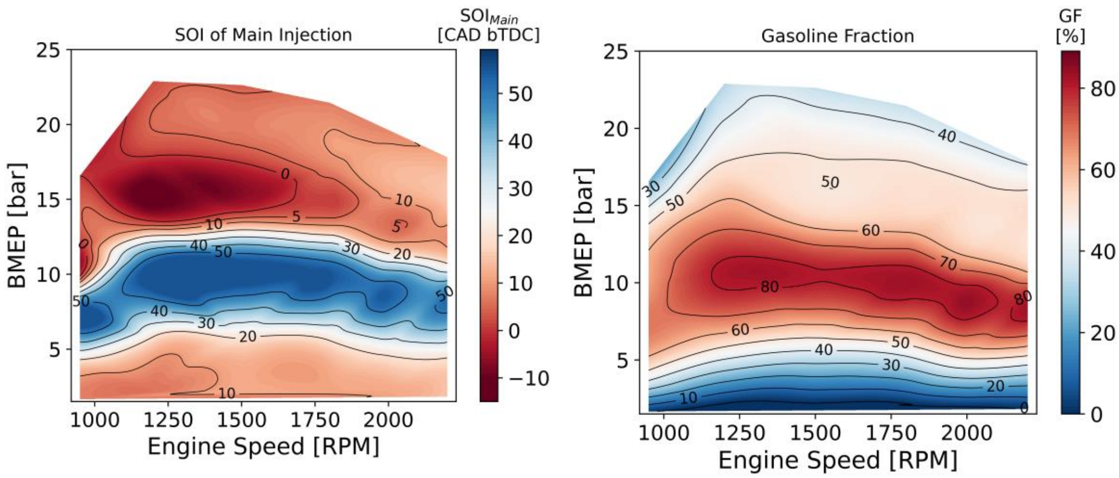

(a) (b)

Figure 5. Evolution of main injection timing (a) and gasoline fraction (b) along the engine map for the DMDF combustion mode.

Considering the observed relation between injection settings and fuel blend with particle formation, a possible conclusion from this qualitative analysis could be that, modifying the engine so that premixed combustion can be extended to higher loads (increasing mechanical resistance, for example), the utilization of higher gasoline fractions and early injections with higher power output could lead to PN levels that could go below currently allowed limits on an engine-out basis.

Although a reduction in particle formation is observed with higher premixing, the levels measured on the RCCI / DMDF combustion are significantly higher than other combustion modes based on premixed combustion like HCCI. This is a complex matter to explain, and a more specific comparison is performed in one of the subsequent sections, but the most relevant aspect to justify the higher particle formation resides in the utilization of a low compression ratio with high EGR rates that significantly increase the concentration of species that can condensate coming from partially oxidized hydrocarbons and also lower the temperature during the exhaust phase. The high concentration of condensates and the low temperatures act as drivers of the nucleation process, giving room for this increase in particle formation compared to other combustion concepts.

From this analysis, it is possible to create a distinction between two clearly differentiated regions along the engine map: a region where particle formation is due to the utilization of high EGR levels that promote condensation of saturated species and, therefore, nucleation processes, and a second region where particles are more related to black carbon classically associated to diffusive combustion. These two particle formation regimes have been classically differentiated by a series of properties, but one of the most common and direct observations would be the size of the particles. Recently nucleated particles coming from the condensation of saturated species are typically characterized by smaller particle sizes, while particles formed of black carbon during diffusive combustion tend to enlarge rapidly. If a characteristic diameter of the particles emitted is computed, a clear trend can be observed. In this case, the Sauter Mean Diameter (D_{32}) was computed according to Eq. 1 since it is a widely accepted parameter to characterize scattered phases where the surface to volume ratio is relevant for mass and energy transfer, like could be the case of a catalyzed DPF. Figure 6 shows how the evolution of the D_{32} has a clear dependency on the combustion mode, resulting in significantly smaller sizes on the RCCI combustion mode used at lower loads. Shorter and leaner combustion processes do not provide the conditions necessary for a significant surface growth of the particles. As the engine load increases and the combustion changes towards a more diffusive strategy, the global particle size increases, showing this change in the relevance of black carbon or soot. In diffusive combustion processes, long residence time within rich pockets of the fuel spray and large concentration of hydrocarbons during the combustion process are favorable conditions for particle growth and aggregation, allowing the formation of significantly larger particles compared to the previous burning conditions.

$$SMD = D_{32} = \frac{\sum N_i \cdot d_i^3}{\sum N_i \cdot d_i^2} \qquad \text{Eq. 1}$$

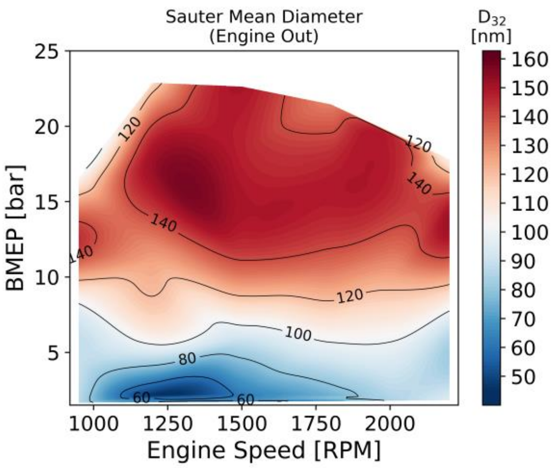

Figure 6. Distribution of global D_{32} of the particle size distribution emitted from the DMDF combustion mode.

An alternative approach to reach the same conclusion is to directly estimate how many particles belong to the nucleation phase and the aggregation phase (enlarged particles, commonly formed of solid black carbon). A well-established rule of thumb used to differentiate between them is to consider a threshold diameter and consider that the particles below that size are mainly formed by particles in the nucleating phase, and the other side of the threshold is dominated by solid particles. The typical value for this threshold is 30 nm, according to the literature [18], which serves the purpose of a rapid comparison. Following this method, for which the complete particle size range from the measurements was considered, the fraction of particles belonging to the nucleating phase is significantly more relevant at lower loads as per Figure 7, and an evident change in the trends is observed as soon as the combustion mode changed towards more diffusive settings. More specifically, a higher fraction of nucleating particles appears in the region where fewer particles were observed in the previous analysis, confirming the influence of premixing and high saturated species concentrations. The presence of potentially-nucleating particles coming from these saturated species drastically diminished for high load conditions where exhaust temperatures are high enough to avoid the condensation of most hydrocarbons.

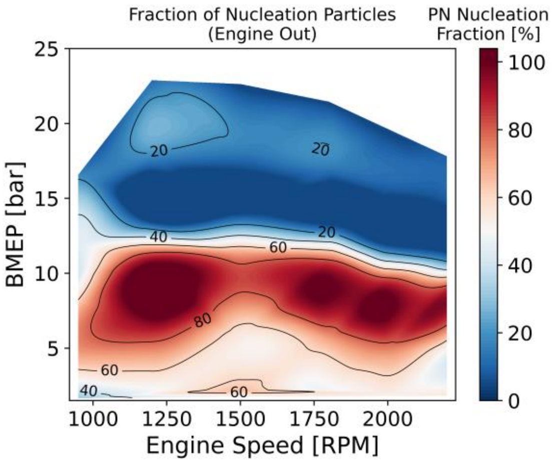

Figure 7. Fraction of particles in the nucleation regime.

The trends highlighted in this section point towards a higher presence of hydrocarbon species that condensate and adhere to the particles or act as nucleating particles, but it is essential to consider that all these results belong to engine-out measurements, and these hydrocarbon species are subject to be oxidized after passing through the DOC. For this reason, a more detailed analysis of the impact of the catalyst on particle numbering is carried out in the following section.

3.2. Effect of the DOC

Scientists have invested significant efforts to understand and characterize the formation process of particles from combustion processes, and the understanding of the driving mechanisms and how particles are formed and enlarged is well known [32,38,39]. The process can be summarized as follows: partially oxidized species produced during the combustion process, such as unsaturated hydrocarbons, polyacetylenes, and polycyclic aromatic hydrocarbons (PAHs), act as precursors of the soot formation. These precursors undergo a nucleation process in which these gaseous species end up forming polycyclic compounds, also referred to as solid nuclei or black carbon, since they have been dehydrated. Hydrocarbon species can also condensate into liquid particles that are prone to adhere to the solid nuclei in what is known as a growth phase since this does not modify the total number of particles but does enlarge their size. The last step in the particle formation process is referred to as the aggregation phase, in which these enlarged particles can combine and stack with each other leading to large chains of smaller nuclei. This process can go on to form huge particles that can become visible to the naked eye. This formation process with defined phases and characteristic particle shape and composition has been schematized in Figure 8, but more details can be found in the work of Khobragade R. et al. [32] and Mohankumar S et al. [40], from which the graphic has been adapted.

The different particle formation phases are highly dependent on a multitude of factors, like temperature, the composition of the different species involved, or the concentration of particles (liquid and solid). In particular, the number of particles within the nucleation size range and the sizes attained during the growth phase highly depend on the concentration of liquid phase particles (mostly water and saturated hydrocarbons that can condensate at lower temperatures).

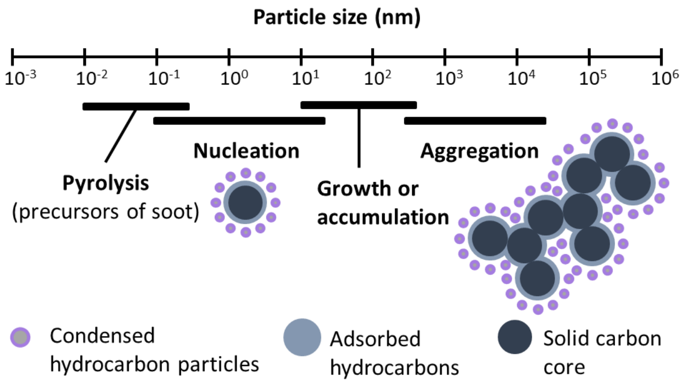

Figure 8. Phases in the particle formation process and characteristic composition (adapted from [32,40]).

This fraction of condensates, also known as the soluble organic fraction (SOF), can constitute a significant fraction not only of the total count of particles but also of the mass contained in these particles. In combustion modes where high EGR rates and low temperatures characterize the working conditions, the high concentrations of partially oxidized hydrocarbons can contribute significantly to increasing the SOF. These condensed species are still subject to be affected when going through a catalyst like the DOC, in which the oxidation of THC and CO is promoted through a series of reactions. Therefore, the effect of the DOC is necessary to define the boundary conditions to other ATS elements like could be a DPF.

Experimental measurements of particles were taken prior to and after the DOC, allowing us to see the reduction of PN due to the reactions that take place in it. Specifically, the reduction in PN was exceptionally high in the region of the map in which high nucleating particles were observed in Figure *7*, showing that the measured particles in this regime might probably consist of a high fraction of liquid particles from the SOF. A more detailed analysis of the evolution of PSD in a characteristic operating condition with moderately high exhaust temperatures shows a significant amount of particles in the range of 8 nm to 30 nm that are reduced by more than one order of magnitude after going through the DOC as shown in Figure 9.

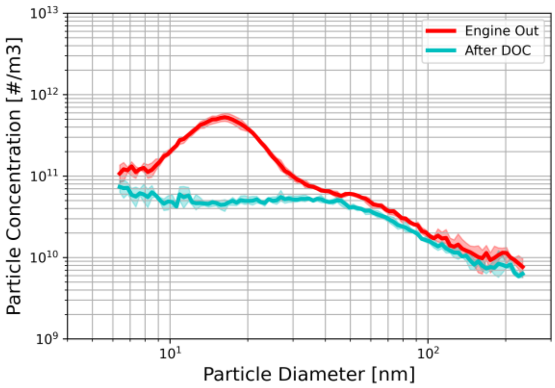

Figure 9. Particle size distribution before and after the DOC at a representative operating condition of the RCCI combustion mode (1200 rpm and 25% load).

In addition to the direct oxidation of SOF due to the effect of the active participation of the DOC, an additional source of particle oxidation was observed at very low load conditions where exhaust temperature is not high enough to light off the DOC. The phenomenon referred to is the NO_2 depletion through the DOC at low temperatures. As Figure 10a shows, NO_2 forms most of the total NOx emissions for these low load conditions, justifying that the concentration of this specie is sufficient to participate in a noticeable rate in catalytic reactions. Figure 10b also represents the region where NO_2 depletion through the DOC is most relevant. This region overlaps with the region of the map where the DOC is still not active due to low temperatures. In this graph, the NO_2 generation coming from high-temperature oxidation of NO was masked to only highlight the relevant region.

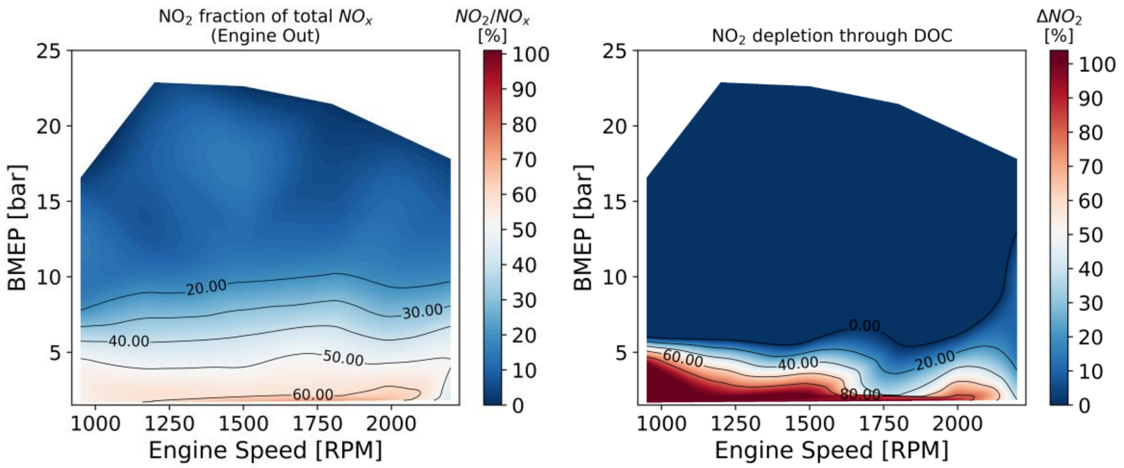

(a) (b)

Figure 10. Distribution of NO2 fraction (a) and NO2 depletion (b) along the DMDF engine map.

This characteristic NO_2 consumption at low temperatures can be attributed to two different phenomena. The first one would be related to the normal catalytic reactions of the DOC to oxidize organic compounds like CO and THC, which in this case could be relevant to explaining the consumption of SOF. To better understand the reactions involved in the balance of NO_2, a reduced chemical reaction model developed by Sampara et al. [41] can be used to evidence the main reactions involved. Eq. 2 considers high-temperature oxidation of NO into NO_2, but as already said previously, this reaction is not of interest for the operating conditions of low load. Eq. 3 and Eq. 4 represent the intervention of NO_2 in the oxidation process of CO and THC at moderate temperatures, and Eq. 5 defines the catalytic dissociation of NO_2 into N_2, which also takes place at moderate temperatures.

$$NO + \frac{1}{2} O_2 \rightarrow NO_2 \qquad \text{Eq. 2}$$

$$CO + NO_2 \rightarrow CO_2 + NO \qquad \text{Eq. 3}$$

$$C_x H_y + \left(2x + \frac{1}{2} y\right) NO_2 \rightarrow xCO_2 + \frac{y}{2} H_2O + \left(2x + \frac{1}{2} y\right) NO \qquad \text{Eq. 4}$$

$$NO_2 \rightarrow \frac{1}{2}N_2 + O_2 \qquad \text{Eq. 5}$$

The second source of NO_2 consumption can be attributed to the passive regeneration of the carbon within the carbonaceous structure of the solid nuclei of particles. This passive regeneration is usually designed to take place at the DPF, but since it is a catalytic oxidation, it can take place at the DOC too. In this case, the reactions can be described by the set of equations included below used by Jeguirim M. et al. [42], in which carbon is oxidized through two simultaneous paths, the direct oxidation with oxygen (Eq. *8* and Eq. *9*) and the oxidation with nitrogen dioxide (Eq. *6* and Eq. *7*).

$$C^* + 2NO_2 \rightarrow CO_2 + 2NO \qquad \text{Eq. 6}$$

$$C^* + NO_2 \rightarrow CO + NO \qquad \text{Eq. 7}$$

$$C^* + NO_2 + \frac{1}{2}O_2 \rightarrow CO_2 + NO \qquad \text{Eq. 8}$$

$$C^* + NO_2 + \frac{1}{2}O_2 \rightarrow CO + NO_2 \qquad \text{Eq. 9}$$

As a result of these potential ways for the DOC to have an impact on the particle distribution, a certain level of emission reduction is observed. Figure 11 includes the particle ratio PN_{ratio} between the outlet and the inlet of the DOC (Figure 11a), which is computed according to Eq. 10, and the total particle count coming out from the DOC (Figure 11b). It is possible to observe that at lower loads, the reduction of PN is most effective, achieving a reduction of nearly an order of magnitude for some conditions, and a good level of oxidation is maintained up to around 50% load, evidencing the characteristic behavior of RCCI combustion with high THC emissions that facilitate the formation of SOF in the particles that are later oxidized in the DOC. At higher loads where the DMDF combustion tends towards the diffusive mode, the SOF fraction is significantly reduced, but a certain level of PN reduction is maintained, implying that the DOC is still acting even on the solid particles.

$$PN_{ratio} = \frac{PN_{out}}{PN_{in}} = \frac{PN_{after\ DOC}}{PN_{engine\ out}} \qquad \text{Eq. 10}$$

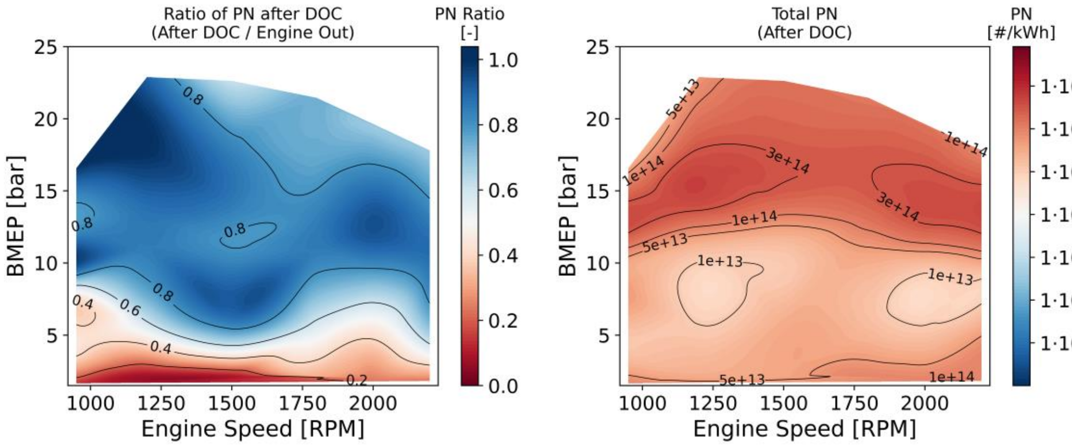

(a) (b)

Figure 11. Evolution of the reduction of PN (a) and total PN after the DOC (b) along the DMDF engine map.

After accounting for DOC oxidation capabilities over the particle distribution, total emissions levels are around an order of magnitude above the regulation for the RCCI regime and significantly higher for DMDF combustion. These results make evident the need to include a DPF. Both interaction paths of NO_2 with SOF and carbon can take place simultaneously, but it is true that both require a certain level of temperature, and a specific residence time in the case of passive regeneration, so it is difficult to differentiate which one has a more significant effect without requiring more fundamental evaluations that fall out of the scope of this investigation. Nonetheless, a clear trend can be observed from the previous figures in which a higher reduction is attained at lower loads by means of oxidation of SOF that represent a higher fraction at lower temperatures due to condensation of THCs, and a certain amount of oxidation is maintained at higher loads where THC condensation cannot occur and most probably the PN reduction is the effect of passive regeneration, although at very low effectiveness ratio due to the short residence time at the DOC.

Considering the requirements for the potential DPF, the DOC provides a reasonable reduction of particles at lower loads, while for higher loads, the NO_2 production coming from the catalytic reactions facilitates the enhancement of the performance of the DPF, in which particles are trapped to increase residence time and allow a more significant passive regeneration [43]. Also, the reduction of smaller particles through the DOC reduces the demand on the DPF by increasing the global size of particle distribution, as seen in Figure 12. In general, the particle distributions at high load with diffusive strategies have not changed practically since large, and carbonous particles with low content of volatile species are not affected significantly by the effect of the DOC. On the contrary, in low load conditions where hydrocarbon species implied a significant fraction of the particle volume, after the oxidation of these species through the DOC, a significant amount of particles in the nucleating regime were reduced since they mostly had adsorbed condensed hydrocarbons that were easily oxidized through surface reactions. This implied that larger particles remain and the global size of the particle distribution is enlarger, facilitating a design of the DPF capable of capturing most of the particles on the larger side of the distribution [44]. Also, as an alternative to the dual elements, it is possible to use a simplified ATS with a single component that includes the effects of a DOC and a DPF in a single component, enhancing performance and reducing complexity and costs [45].

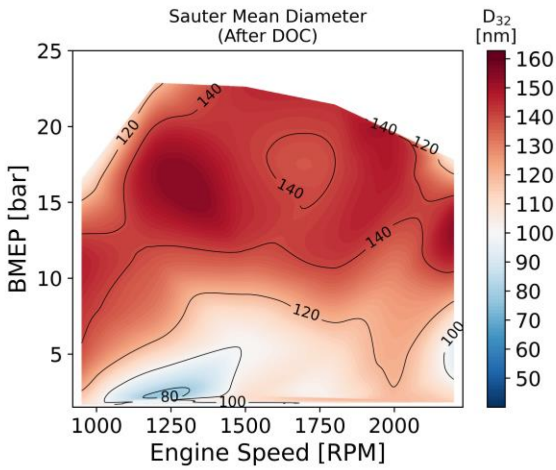

Figure 12. Distribution of D32 after the DOC along the DMDF engine map.

Combining the data from Figure 11 and Figure 12, the requirements for the necessary DPF can be defined. The concentrations of particles that the DPF will consider can range from slightly less than 10^{13} up to 10^{14} #/kWh depending on the operating conditions, and the characteristic SMD of the particle size distribution can range from 80 up to 160 nm. The most demanding conditions for the DPF will be under RCCI combustion mode since smaller particles may require smaller corridors in the matrix, but for a proper assessment, a dedicated design procedure should be considered in future steps.

3.3. Particle size distribution and modal analysis

After analyzing the global properties of the particles emitted under DMDF combustion and observing the impact of the DOC on the concentration of particles, a clear differentiation in the trends is observed depending on the particle size. To better observe these differences in composition and concentration along with the different combustion modes, it is of interest to analyze the PSD and how they are modified through the DOC. Figure 13 depicts the PSD of three dominant and characteristic combustion modes of the current application. The PSDs shown in Figure 13 belong to a single engine speed (1500 rpm), but the analyzed trends are maintained for the rest of the engine loads despite the effect of different engine speeds and operating temperatures that modify the global size tendency of the PSD slightly.

The first mode in Figure 13a would be the RCCI combustion at low loads (1 to 5 bar of BMEP), in which low-temperature combustion with high EGR rates dominates. A clear dominant group of particles falls within the smaller size, characterized by nucleating particles that are more volatile. The change of the PSD after going through the DOC clearly shows how this specific region is significantly reduced, implying the presence of volatile compounds that are oxidized by the DOC, achieving a reduction of more than an order of magnitude. At larger particle sizes, the presence of volatile particles is almost negligible, and no significant reduction is observed as a consequence of the difficulty of reducing solid particles (soot). Nonetheless, these larger particles represent a relatively small fraction of the total particle count.

As load is increased (up to 12 to 14 bars of BMEP) and high premixing accompanied by higher utilization of gasoline is employed, a significant modification of the PSD characteristics can be observed in Figure 13b. The global concentrations are slightly increased, with very similar trends at the aggregation regime, but in this region, the relevance of the nucleating particles is significantly smaller. Also, the reduction capacity of these smaller particles has been significantly limited since the high temperatures at these loads impede the condensation of THCs. Small nuclei are still being formed, but the dominating mechanism is related to solid carbonaceous nuclei instead of particles that have grown with adsorbed liquid hydrocarbons. A consequence of this limited growth is that the average size of the nucleating particles is even smaller than in the previous combustion mode. Despite this reduced relevance of the nucleating regime, it still is the most relevant regime through the measured particle size range.

Higher engine loads (up to 25 bar BMEP), represented by the PSD shown in Figure 13c, are dominated by the dual-fuel diffusive combustion, characterized by latter HRF injections and richer mixture formation. Due to these combustion conditions, the trends in the PSD are entirely different. Global particle concentrations are significantly greater than in the previous combustion modes, mainly driven by the shorter oxidation time within the cylinder and the rich burning ambient, which promotes great particle formation. The aggregated fractal particles take the leading role, enlarging the global size of the particles emitted while the nucleating regime maintains similar concentrations to the previous premixed combustion mode. In general, temperatures are sufficiently high to avoid any condensation, and practically no particle reduction is observed clearly for this combustion strategy. Nonetheless, as observed in Figure 9, some reduction is still taking place within the DOC, most probably driven by passive regeneration of carbonaceous matter with NO_2 since it is highly reactive at the given operating temperatures. Regardless, the effectiveness of these reduction mechanisms is limited by low residence times and other potentially dominant reactions over NO_2 concentration.

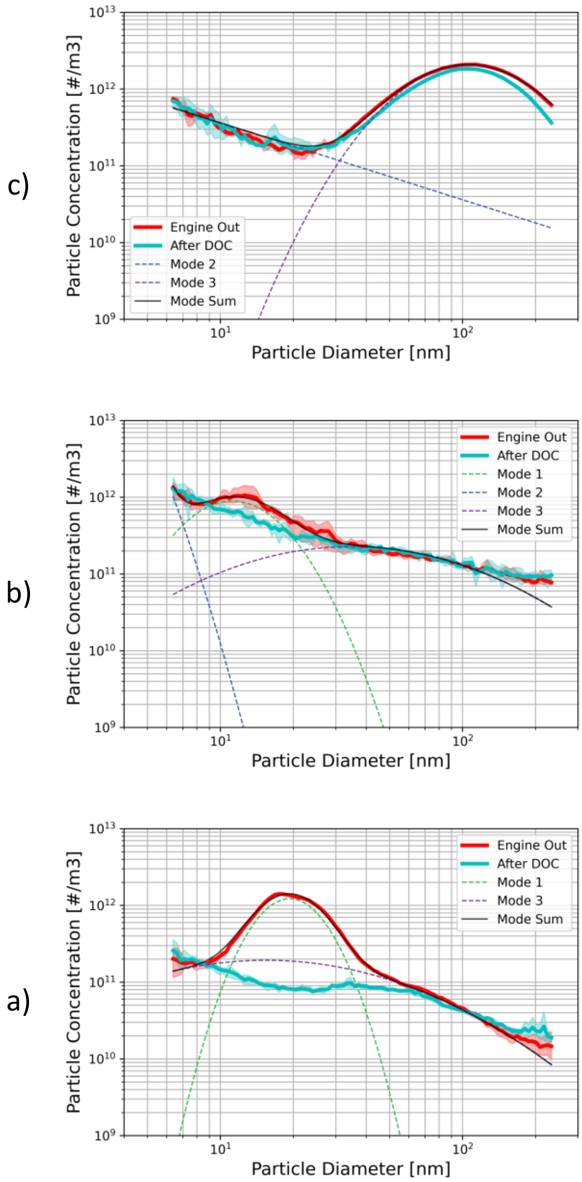

Figure 13. Particle Size Distribution before and after DOC at low (a), medium (b), and high (c) engine loads.

In addition to the measured PSD from the engine exhaust and the DOC outlet, a multi-log-normal fitting was applied to these particle distributions (only to engine out distributions) to identify additional particle modes [46]. Particle formation during combustion can occur through different physicochemical paths, and nuclei can be formed from different sources, so it is possible to observe primary particles (smaller nuclei) that form different modes or distributions [47]. Conventional combustion modes are typically characterized by two main modes, related to volatile nucleating particles and solid aggregated particles [32,38,40,48].

The low load RCCI combustion showed this apparent trend of two differentiated modes associated with classical particle modes: mode 1 for volatile nuclei and mode 3 for solid aggregated particles. Similarly, diffusive combustion also shows this bimodal behavior, but volatile nuclei (mode 1) are substituted by solid primary particles since they are not easily oxidized or vaporized (mode 2), meaning that no SOF is present in these particles.

An interesting behavior appears in the highly premixed combustion mode for moderate loads, in which a tri-modal behavior can be observed. Volatile particles from mode 1 and solid smaller nuclei from mode 2 coexist with similar relevance for the total particle distribution while maintaining the presence of aggregated particles from mode 3. These small non-volatile primary particles fall way below the range considered for the current EURO VI regulation or the prospective range for the future EURO VII [2,49], so the impact on the total count of particles is minimum, but this differentiated behavior in the formation of particles can result of interest when analyzing the relevance of other sources of particle formation apart from fuel combustion, like oil pyrolysis or metal depositions [50,51] for future technological improvements.

3.4. Estimation of Particulate Mass

In addition to total particle numbering, the current normative also considers total particulate mass emitted by the engine [2]. Therefore, to adequately characterize particle emissions from the DMDF combustion, it is necessary to cover this aspect. Although there exists specific measurement equipment for directly quantifying the particle mass in the exhaust line, a common practice when not available is to define a density of particle and compute volume and mass based on the particle diameter. For smaller and spherical particles that have not gone through the aggregation process, the density of the particle based on its mobility diameter is equal to the density of the material of the particle, but particles that have aggregated and branched into fractal structures tend to have a mobility diameter greater than the associated to the volume of the material, so it is necessary to account for this fractal structure with void gaps. This relationship between effective density and mobility diameter can adequately be described by a power law with the expression of Eq. 11, in which d_m is the particle mobility diameter, D_m is the mass-mobility exponent accounting for fractal structures, and C is a fitting constant to match the reference density.

Other studies show a clear dependency between particle density and fuel composition. In the work of Ouf et al., a wide variety of fuels were tested to evaluate the effective density of the particles they produced [52]. Works like the one from Momenimovahed et al. [53] provide correlations for the effective particle density as a function of its diameter and the substitution rate in a diesel-natural gas engine. Considering these works, it is adequate to consider that in the current work, the blend of gasoline and diesel is changed for all operating conditions. An effective particle density can be defined by considering two different particle density correlations for both fuels and weighting them based on the mass fraction distribution of the fuel input as in Eq. 12.

$$\rho_p = C \cdot d_m^{D_m - 3} \qquad \text{Eq. 11}$$

$$\rho_{eff} = GF \cdot \rho_{LRF} + (1 - GF) \cdot \rho_{HRF} \qquad \text{Eq. 12}$$

The correlations for particles emitted by the LRF and the HRF are obtained from the literature. A bibliographic review was carried out to find recent studies for diesel and gasoline under working conditions similar to the ones used for this study. Fuel composition advancements, low-temperature combustion modes, low compression ratio, and high premixing ratios are factors that have been introduced in recent years, and all of them have their impact on particle structure and composition. In the case of HRF, the work from A. Momenimovahed et al. [53,54] studied particle emissions for diesel and diesel-CNG blends under low-temperature combustion modes with significant premixing ratios, and the work from A. Zelenyuk et al. [55] investigated particulate mass and numbering on a GCI engine, providing a density correlation used for the gasoline part in this study. Both density evolutions with particle diameter are represented in Figure 14.

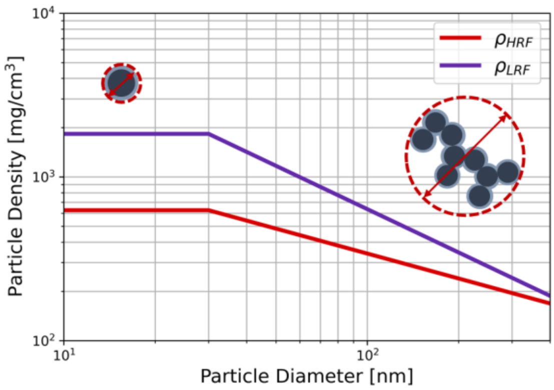

Figure 14. Density correlations used for HRF and LRF.

The total particulate mass emitted is computed by considering the particle volume based on its mobility diameter and the effective density previously described using the cumulative expression from Eq. 13.

$$PM = \int \rho_{eff} \frac{\pi}{6} d_m^3 \frac{dN}{d \log d_m} d \log d_m \ = \sum \rho_{eff,i} \frac{\pi}{6} d_i^3 N_i \qquad \text{Eq. 13}$$

For soot mass emissions, the installations also included a smoke meter that measures gas opacity according to the blackening of a calibrated filter, which is then converted to solid mass using a correlation provided by the manufacturer. This is a widely used technique to measure soot mass and was also included in the study. The differences in both methods for obtaining particle mass may lead to differences in the reported value. FSN measurements do not deal appropriately with particles in the ultrafine regime since they do not produce sufficient darkening of the filter. Although the total mass represented by these fine particles is minimal, it is evident that FSN measurements always underpredict total mass under conditions with very low emissions of soot. On the other hand, FSN measurements include all the range of possible particles in the exhaust, so the larger particles that actually have a significant impact on total mass are considered. The pass estimation using the PSD is limited to only the measured range of particle size, so any particles that may fall out of this range, especially the large particles over the upper measured limit, are not considered. For this reason, the PSD method tends to underestimate total mass when large particles are present slightly.

Despite these potential discrepancies, the comparison between both estimations leads to a good alignment of the reported values for values above 10 mg/kWh. Figure 15 shows how both approaches do align in the final values of PM, having the most considerable misalignment on the small values, as explained before. The fact that the under prediction of total mass by the PSD approach on the cases with high soot mass is relatively small implies that the number of particles missed by the measuring range is small and that the values reported are sufficiently trustable as an estimation. Also, it can be inferred that the analysis of particle properties and distributions accounted for most of the relevant particle modes.

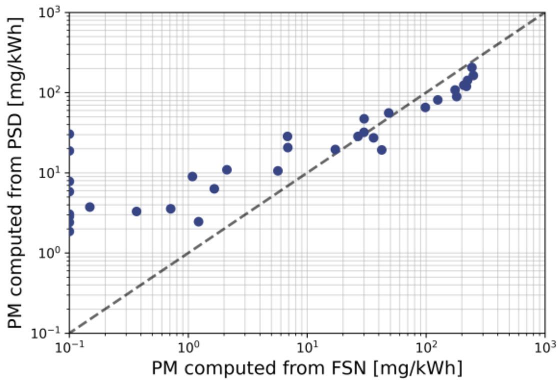

Figure 15. Comparison of the PM estimation with FSN and PSD measurements.

The final reported values of total PM reported from the PSD approach are shown in Figure 16, differentiating between engine out measurements and post-DOC measurements. The results show how the RCCI combustion mode used up to 50% load is capable of producing ultra-low soot emissions, with further reduction after the DOC thanks to the oxidation of volatile species that had condensed. This allows fulfilling the EURO VI regulation of PM up to 50% engine load without needing a specific concern on this aspect. On the diffusive side of the map, the production of larger particles implies that total soot mass is also increased, and this is reflected in the reported values that do not fulfill the regulation limit anymore. Nonetheless, the values of soot mass are within the typical range of emission levels from other engine concepts with similar injection strategies, and the design of conventional after-treatment devices is sufficient to deal with this level of solid mass. It is worth mentioning that the maximum values of PM are achieved just at the limit at which NOx emissions do still fulfill the EURO VI limit. This is a dependency of both species emissions with EGR level and air-to-fuel ratio. A design of the turbocharging system that allows maintaining EGR with leaner conditions could potentially maintain NOx levels while significantly mitigating soot emissions [56]. Other modifications of the architecture, like piston bowl design or the aim of extending the RCCI combustion mode by improving mechanical resistance, can also improve the concept to lower soot production [57,58].

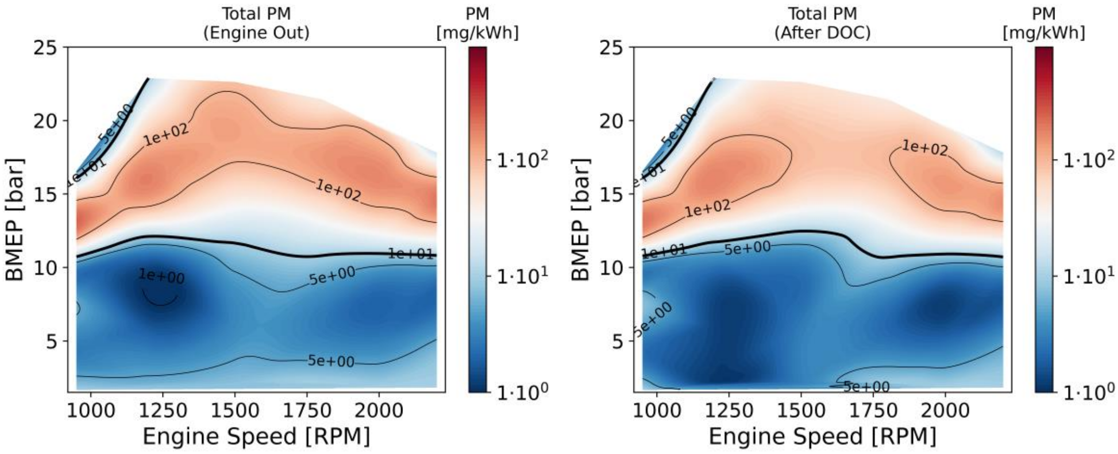

(a) (b)

Figure 16. Distribution of PM emissions from the engine (a) and after the DOC (b) along the DMDF engine map.

3.5. Technological positioning of the DMDF engine

With the objective of positioning the results obtained in this study with other existing technologies for internal combustion engines, a bibliographic review was carried out to picture the current alternatives and status in terms of particle numbering and particulate mass emissions. The data from Hallquist et al. [59] on heavy-duty applications with conventional diesel combustion and compressed natural gas (CNG), together with the data from Khalek I. et al. [60,61] on CNG heavy-duty applications, was used to picture current commercial alternatives for CI engines. Prikhodko V. et al. [62]

and Zhang Y. et al. [63] carried out thorough comparisons of different technologies that cover concepts like CDC, CDC with low-temperature combustion modes based on high dilution with EGR, CNG, RCCI fueled with Diesel-Gasoline and Diesel-CNG fuel combinations and Gasoline Compression Ignition (GCI). The works from Bock N. et al. [64] and Omar I. et al. [65] provided a complete review of the status of spark ignition (SI) engines on a variety of configurations with PFI and DI injection systems [66,67]. Lastly, the recent work from Gelner A. et al. [23] states how advanced oxygenated fuels can improve particle emissions.

In order to provide a more realistic performance indicator of the technology evaluated in this work, a global emission factor was obtained by numerically interpolating through the different engine maps produced during this study following the engine speed and engine load profiles defined for the World Harmonized Transient Cycle (WHTC) engine homologation cycle using the numerical tools described in previous works from the authors [57,68,69]. In order to differentiate between pure RCCI combustion mode and the DMDF multi-mode engine map, the engine load profile was scaled to a maximum engine load of 50% to capture the performance of pure RCCI combustion that could be characteristic of de-rated versions of the same engine on less demanding applications, and the complete engine map was utilized to provide the global performance of the DMDF combustion mode. The effect of the DOC was also captured and represented in the results.

The global status and the comparison of the different mentioned technologies were compiled in Figure 17. In this image, the scattered data was used to fit a bivariate normalized regression to produce the ellipses that represent the area with a confidence level of 3σ, a typical value for representative intervals. From this image, it is clear that current CDC engines, independently of whether they use high EGR levels to control other pollutant species or not, are the ones with the worst performance in terms of PM and PN. Aftertreatment systems with a DPF are a practical solution, although not perfect for these applications. The other technologies progressively improve towards lower PM and PN engine-out emissions as we move through CNG, RCCI, GCI, and HCCI combustion modes applied on CI engines. SI engines have the particularity of producing ultra-low PM emissions with moderate and low PN levels. Nonetheless, they still require some ATS devices like the GPF (Gasoline Particulate Filter) to reach homologation conditions. On the extreme of advanced alternative fuels, polyoxymethylene dimethyl ethers (OME) has proved to reduce particle emissions successfully thanks to the lack of carbon-to-carbon bonds in their molecular structure [70], not needing any ATS dedicated device for particle emissions control.

From the positioning of the results obtained for the RCCI combustion in the present work, it can be seen that PM levels are successfully below the allowed limits, but PN levels are on the moderately high side. Compared to other RCCI studies, the current configuration employs low-pressure EGR and targets to reach EURO VI levels of NOx and zero FSN readings, or what is the same, ultra-low PM emissions. By targeting these two contaminants simultaneously, higher PN levels are emitted by high EGR levels, low temperatures, and high concentrations of hydrocarbons that can condensate and nucleate, as already proven. Resulting PN and PM levels for the RCCI in this work can be considered to be near GCI and SI conditions. On the other hand, the DMDF combustion mode is characterized by highly diffusive dual-fuel combustion strategies with high EGR levels, producing relatively richer combustion conditions. It is no surprise to see that PN and PM levels are similar to those of modern CDC engines with LTC strategies. For both cases, the effect of the DOC contributes to mitigating both mass and number of particulate emissions, especially on the RCCI combustion as previously studied, achieving a reduction of PN of almost an order of magnitude.

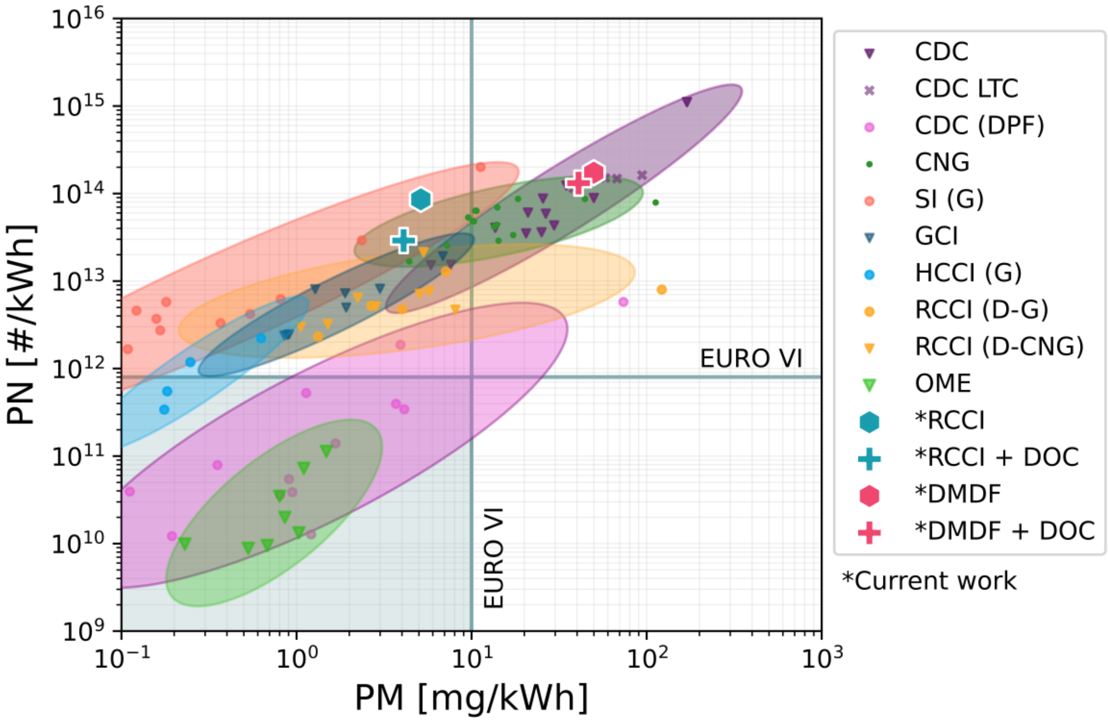

Figure 17. Comparison of different combustion modes in terms of PN and PM specific emissions.

Considering the DOC outlet conditions, the RCCI engine delivers a global particle distribution of $2.9 \cdot 10^{13}$ #/kWh in BSPN and 4.1 mg/kWh in BSPM, with an average SMD of roughly 92 nm. With the extended engine map using the DMDF combination, these numbers grow up to $1.3 \cdot 10^{14}$ #/kWh, 40.8 mg/kWh, and 108 nm for BSPN, BSPM, and SMD, respectively. Particle mass and concentration have been increased by a factor of 10, and global particle size was enlarged by 10%. It is evident that a dedicated device for controlling particulate emissions is required in the simplified ATS for the RCCI combustion mode, but the specifics of the design may vary significantly. Considering the previous graph, it could be possible to state that since RCCI combustion mode delivers PN and PM levels similar to those of SI and GCI [71], a particulate filter under a design similar to modern GPF would be suitable, but it is necessary to consider the operating conditions for the filter. Gasoline engines do have much higher exhaust temperatures and significantly higher flow rates due to the difference in engine regime. The filters for these applications are usually made out of cordierite since it is more thermally resistant, and the ceramic matrix is designed to limit the backpressure that increases with flow rates, compromising filtering/trapping capacity with a higher porosity level (larger gaps) since the PN levels that have to work with are in the moderate to low side. Thanks to the high exhaust temperatures, active regeneration is easily triggered, and an effective solution is reached [72]. On the other hand, diesel applications do have lower mass flows and exhaust temperatures, allowing to change to silicon carbide ceramic matrixes and tighter cell design, significantly improving filtering/trapping efficiency throughout all the particle size domains and higher passive regeneration on catalyzed DPFs [73–75]. Nonetheless, to trigger active regeneration of the trapped particles, dedicated post-injection strategies of direct injection in the exhaust line may be required to achieve the needed temperatures.

Both RCCI and DMDF configurations do have lower exhaust temperatures and mass flows compared to conventional diesel engines since the high EGR levels displace a significant amount of fresh air. Considering this, a filter design more similar to that of DPFs would be more successful in reducing particle emissions down to the allowed levels. The specifics of the design may slightly differ since the dominant particle sizes to trap are different, but the backpressure limitation may not be a hard limitation for these applications, allowing for more compact filtering systems. Assuming that a proper filter design can provide ultra-low levels of PM and PN on the DMDF combustion mode, this technology would prove to be incredibly attractive as a substitute for conventional diesel engines since engine efficiency has been proven to be increased, NOx emissions do not need dedicated ATS, and a conventional DOC is more than capable of reducing the high levels of CO and THC emissions [76], resulting in a more efficient engine capable of covering the whole operating range of the engine with a reduced ATS system without SCR nor urea injection.

An alternative to using dedicated filtering devices is the utilization of alternative fuels. As stated in the previous comparison, advanced synthetic fuels with controlled chemical composition allow having no carbon-to-carbon bonds in the molecular structure of the fuel, mitigating the formation of polycyclic hydrocarbons that act as precursors of soot formation. The particle measurements from other scientists combined with previous studies of the authors that studied the utilization of OMEx as HRF in the DMDF engine with ultra-low soot readings throughout the complete engine map [57] suggest that this alternative could potentially result in an architecture that would only require a single DOC to fully oxidize CO and THCs. NOx levels could be reduced down to half of the currently allowed limits and with a CO_2 footprint that can reach up to a 50% reduction in the well-to-wheel (WtW) perspective [77]. Nonetheless, dedicated studies on PN emissions from such a combination would be required to confirm this statement.

4. Conclusions and future work

The present work studied the particulate emissions of an adapted medium-duty engine working under a dual-mode dual-fuel combustion concept aiming to maintain ultra-low NOx emissions and very low soot production on the RCCI combustion mode. An experimental evaluation was carried out considering the effects of a DOC in the exhaust line to define the working conditions of a potential filter, and a comparison against other technologies was provided. Out of the results and analyses carried out, the following main conclusions were obtained:

- The current concept results in ultrafine particle emissions when working on RCCI premixed mode, having a significant fraction of particles nucleated from or grown by condensed hydrocarbon species and ranging in sizes between 5 nm and 40nm. On the diffusive injection strategies, larger particles of around 80 nm to 200 nm formed of solid black carbon are formed due to richer conditions and higher temperatures that do not allow phase change of gaseous species.
- The DOC allows for a reduction of up to 90% of the particle concentrations produced by the RCCI mode, and a limited reduction is observed on solid particles. The reduction mechanisms actuating on the oxidation of particles have been associated with both: pure oxidation of THCs at moderately high exhaust temperatures and passive regeneration of soot through NO_2 interaction at low temperatures where the DOC is still not lighted off.
- The dedicated analysis of the PSD allowed us to see how as the combustion strategies change with the engine load, the dominant nucleating modes change and produce bi-modal and tri-modal distributions depending on the engine operating condition. The characterized particle distributions directly emitted by the engine had a global SMD that ranged from around 60 nm in RCCI up to 160 nm in DMDF mode.
- The evaluation of global performance on a simulated homologation cycle yields a characteristic particulate emission of $2.9 \cdot 10^{13}$ #/kWh in BSPN and 4.1 mg/kWh

in BSPM with an average SMD of roughly 92 nm when operating on RCCI mode. These levels a very similar to those of GCI and SI, so a relatively simple filtering system could allow reaching the required, acceptable values. These numbers increased by a factor of 10 for the DMDF, making it very similar to a CDC application.

- The current status of the DMDF concept allows reaching EURO VI levels engine out of NOx. CO and THC are successfully oxidized with a conventional DOC, and a filtering system similar to that of diesel engines would be sufficient to reach ultra-low levels of PN and PM.

The results from this study have characterized the inlet conditions and requirements for a DPF that is suitable for the DMDF application, considering particle numbering, size distribution, SMD, and total mass. These values can be used in future investigations to properly define suitable filtering devices that can deal with the ultrafine particles of the RCCI or the high concentration levels of the DMDF, depending on the application contemplated. By having detailed PSDs, adequate filtering efficiencies and a proper assessment of potential back pressure can be obtained during the design process.

The consideration of advanced alternative fuels within the comparison carried out in this work highlighted the potential of OMEx to highly reduce particle formation. Previous studies from the same research group on this study suggest that this also applies to DMDF when using OMEx as HRF; therefore, an interest in validating this technology with synthetic fuels can motivate to carry out a dedicated evaluation of particle emissions targeting prospective future levels of emission on an engine fueled with OMEx and Gasoline in the future.

Acknowledgments

The authors thank ARAMCO Overseas Company and VOLVO Group Trucks Technology for supporting this research. This research work has been partially supported by Grant PDC2021-120821-I00 funded by MCIN/AEI/10.13039/501100011033 and by European Union NextGenerationEI/PRTR. The authors acknowledge the Conselleria de Innovación, Universidades, Ciencia y Sociedad Digital de la Generalitat Valenciana for partially supporting this research through grant number GV/2020/017.

References

[1] GHG emissions by main sector in the EU-28, 1990-2017 n.d.

[2] European Parliament And The Council Of The European Union. Regulation (EC) No 595/2009 of The European Parliament and of the Council of 18 June 2009 on type-approval of motor vehicles and engines with respect to emissions from heavy duty vehiclec (Euro VI) and amending Regulation (EC) No 715/2007 and Directive 20 2018;52:48–119.

[3] Bell L, Spinler S, Winkenbach M. Economic, social and ecological impact assessment of mixed light rail, battery-electric vehicles, fuel cell-electric vehicles and electrified cargo bikes in urban environment of advanced integrated simulation approach. SSRN Electronic Journal 2022;43:2086–107. https://doi.org/10.2139/ssrn.4011273.

[4] Sanguesa JA, Torres-Sanz V, Garrido P, Martinez FJ, Marquez-Barja JM. A Review on Electric Vehicles: Technologies and Challenges. Smart Cities 2021;4:372–404. https://doi.org/10.3390/smartcities4010022.

[5] Tchouvelev A v., de Oliveira SP, Neves NP. Regulatory Framework, Safety Aspects, and Social Acceptance of Hydrogen Energy Technologies. Science and Engineering of Hydrogen-Based Energy Technologies, Elsevier; 2019, p. 303–56. https://doi.org/10.1016/B978-0-12-814251-6.00006-X.

[6] Luis F, Moncayo G. Reaching net-zero carbon emissions from harder-to-abate sectors by mid-century. n.d.

[7] Wang Y, Wang J, Hao C, Wang X, Li Q, Zhai J, et al. Characteristics of instantaneous particle number (PN) emissions from hybrid electric vehicles under the real-world driving conditions. Fuel 2021;286:119466. https://doi.org/10.1016/j.fuel.2020.119466.

[8] Krishnamoorthi M, Malayalamurthi R, He Z, Kandasamy S. A review on low temperature combustion engines: Performance, combustion and emission characteristics. Renewable and Sustainable Energy Reviews 2019;116:109404. https://doi.org/10.1016/j.rser.2019.109404.

[9] Benajes J, García A, Monsalve-Serrano J, Villalta D. Exploring the limits of the reactivity controlled compression ignition combustion concept in a light-duty diesel engine and

the influence of the direct-injected fuel properties. Energy Conversion and Management 2018;157:277–87. https://doi.org/10.1016/j.enconman.2017.12.028.

[10] Benajes J, García A, Monsalve-Serrano J, Sari R. Clean and efficient dual-fuel combustion using OMEx as high reactivity fuel: Comparison to diesel-gasoline calibration. Energy Conversion and Management 2020;216:112953. https://doi.org/10.1016/j.enconman.2020.112953.

[11] Zhang Z, Li J, Tian J, Zhong Y, Zou Z, Dong R, et al. The effects of Mn-based catalysts on the selective catalytic reduction of NOx with NH3 at low temperature: A review. Fuel Processing Technology 2022;230:107213. https://doi.org/10.1016/j.fuproc.2022.107213.

[12] Ragon AP, Rodríguez F. Estimated cost of diesel emissions control technology to meet future Euro VII standards 2021:1–27.

[13] Giechaskiel B, Schiefer E, Schindler W, Axmann H, Dardiotis C. Overview of soot emission measurements instrumentation: From smoke and filter mass to particle number. SAE International Journal of Engines 2013;6:10–22. https://doi.org/10.4271/2013-01-0138.

[14] Wu B, Deng L, Gu W, Wu B, Guo J. Experimental investigation of combustion and particle emissions under different combustion modes on a heavy-duty diesel engine fueled by diesel/gasoline/diesel from direct coal liquefaction. Fuel 2019;254. https://doi.org/10.1016/j.fuel.2019.115661.

[15] Giechaskiel B, Melas A, Martini G, Dilara P, Ntziachristos L. Revisiting Total Particle Number Measurements for Vehicle Exhaust Regulations. Atmosphere (Basel) 2022;13:1–36. https://doi.org/10.3390/atmos13020155.

[16] Saxena MR, Maurya RK. Influence of direct injection timing and mass of port injected gasoline on unregulated and nano-particle emissions from RCCI engine. Fuel 2020;282:118815. https://doi.org/10.1016/j.fuel.2020.118815.

[17] Zhang Y. Comparisons of Particulate Size Distributions from Multiple Combustion Strategies 2017.

[18] Bermúdez V, García A, Villalta D, Soto L. Assessment on the consequences of injection strategies on combustion process and particle size distributions in Euro VI medium-duty diesel engine. International Journal of Engine Research 2020;21:683–97. https://doi.org/10.1177/1468087419865652.

[19] Benajes J, García A, Monsalve-Serrano J, Boronat V. Gaseous emissions and particle size distribution of dual-mode dual-fuel diesel-gasoline concept from low to full load. Applied Thermal Engineering 2017;120:138–49. https://doi.org/10.1016/j.applthermaleng.2017.04.005.

[20] Zhang Z, Li J, Tian J, Dong R, Zou Z, Gao S, et al. Performance, combustion and emission characteristics investigations on a diesel engine fueled with diesel/ ethanol /n-butanol blends. Energy 2022;249:123733. https://doi.org/10.1016/j.energy.2022.123733.

[21] Macián V, Monsalve-Serrano J, Villalta D, Fogué-Robles Á. Extending the potential of the dual-mode dual-fuel combustion towards the prospective EURO VII emissions limits

using gasoline and OMEx. Energy Conversion and Management 2021;233. https://doi.org/10.1016/j.enconman.2021.113927.

[22] Zhang Z, Tian J, Li J, Lv J, Wang S, Zhong Y, et al. Investigation on combustion, performance and emission characteristics of a diesel engine fueled with diesel/alcohol/n-butanol blended fuels. Fuel 2022;320:123975. https://doi.org/10.1016/j.fuel.2022.123975.

[23] Gelner AD, Rothe D, Kykal C, Irwin M, Sommer A, Pastoetter C, et al. Particle emissions of a heavy-duty engine fueled with polyoxymethylene dimethyl ethers (OME). Environmental Science: Atmospheres 2022;2:291–304. https://doi.org/10.1039/d1ea00084e.

[24] Zhang Z, Tian J, Li J, Cao C, Wang S, Lv J, et al. The development of diesel oxidation catalysts and the effect of sulfur dioxide on catalysts of metal-based diesel oxidation catalysts: A review. Fuel Processing Technology 2022;233:107317. https://doi.org/10.1016/j.fuproc.2022.107317.

[25] Systems EM. Emission Measurement Systems - HORIBA 2019:1–3.

[26] AVL. Smoke Value Measurements with the Filter-Paper-Method. 2005.

[27] Testo. testo MD19-3E User Manual. n.d.

[28] Incorporated TSI. Model 3936 Scanning Mobility Particle Sizer (SMPS) Spectrometer Instruction Manual 2008:1–83.

[29] Payri F, Olmeda P, Martin J, Carreño R. A New Tool to Perform Global Energy Balances in DI Diesel Engines. SAE International Journal of Engines 2014;7:2014-01–0665. https://doi.org/10.4271/2014-01-0665.

[30] Petitpas G, Whitesides R, Dernotte J, Dec J. Refining Measurement Uncertainties in HCCI/LTGC Engine Experiments. SAE Technical Papers 2018;2018-April:1–12. https://doi.org/10.4271/2018-01-1248.

[31] Benajes J, García A, Monsalve-Serrano J, Sari R. Clean and efficient dual-fuel combustion using OMEx as high reactivity fuel: Comparison to diesel-gasoline calibration. Energy Conversion and Management 2020;216:112953. https://doi.org/10.1016/j.enconman.2020.112953.

[32] Khobragade R, Singh SK, Shukla PC, Gupta T, Al-Fatesh AS, Agarwal AK, et al. Chemical composition of diesel particulate matter and its control. Catalysis Reviews - Science and Engineering 2019;61:447–515. https://doi.org/10.1080/01614940.2019.1617607.

[33] Wyslouzil BE, Wölk J. Overview: Homogeneous nucleation from the vapor phase - The experimental science. Journal of Chemical Physics 2016;145. https://doi.org/10.1063/1.4962283.

[34] Kasper M. The number concentration of non-volatile particles - Design study for an instrument according to the PMP recommendations. SAE Technical Papers 2004;2004. https://doi.org/10.4271/2004-01-0960.

[35] Fuentes López E. Caracterización de la influencia de las condiciones de operación de motor sobre la distribución de tamaños de las partículas diesel. 2006.

[36] Soto Izquierdo L. Estudio del efecto de diferentes estrategias de formación de la mezcla sobre las emisiones gaseosas y de partículas en nuevos conceptos de combustión de motores de encendido por compresión 2020:52–6.

[37] Wiedensohler A, Birmili W, Nowak A, Sonntag A, Weinhold K, Merkel M, et al. Mobility particle size spectrometers: Harmonization of technical standards and data structure to facilitate high quality long-term observations of atmospheric particle number size distributions. Atmospheric Measurement Techniques 2012;5:657–85. https://doi.org/10.5194/amt-5-657-2012.

[38] Kittelson D, Kraft M. Particle Formation and Models in Internal Combustion Engines. Cambridge Centre for Computational Chemical Engineer 2014:1–39.

[39] Park S, Shin JY, Bae C, Jung J, Lee J. Combustion phenomena affecting particle emission under boosting conditions in a turbocharged gasoline direct injection engine. Fuel 2021;286:119362. https://doi.org/10.1016/j.fuel.2020.119362.

[40] Mohankumar S, Senthilkumar P. Particulate matter formation and its control methodologies for diesel engine: A comprehensive review. Renewable and Sustainable Energy Reviews 2017;80:1227–38. https://doi.org/10.1016/j.rser.2017.05.133.

[41] Desai C, Kadam V, Chowdhury K, Sampara C, Chemicals V, Limited P. 2022-Global Kinetic Modeling of a Commercial DOC Based on a Reduced Synthetic Gas Bench Protocol 2022:1–9. https://doi.org/10.4271/2022-01-0558.Received.

[42] Jeguirim M, Tschamber V, Brilhac JF. Kinetics of catalyzed and non-catalyzed soot oxidation with nitrogen dioxide under regeneration particle trap conditions. Journal of Chemical Technology and Biotechnology 2009;84:770–6. https://doi.org/10.1002/jctb.2110.

[43] Leistner K, Experimental KL, Study M, Soot D, Leistner K. Experimental and Modelling Study of Catalytic Diesel Soot Oxidation Etude exp' erimentale et mod' elisation de l' oxydation catalys' ee de suies Diesel 2013.

[44] Yang Y, Rutland C, Rothamer D. Study of the Deep-Bed Filtration Using Pore Filtration Model (PFM). SAE International Journal of Fuels and Lubricants 2018;11:287–99. https://doi.org/10.4271/2018-01-0956.

[45] Srinivasan A, Price K. Consolidation of DOC and DPF functions into a single component. SAE Technical Papers 2019;2019-April:1–17. https://doi.org/10.4271/2019-01-0583.

[46] Hussein T, Dal Maso M, Petäjä T, Koponen IK, Paatero P, Aalto PP, et al. Evaluation of an automatic algorithm for fitting the particle number size distributions. Boreal Environment Research 2005;10:337–55.

[47] Kuuluvainen H, Karjalainen P, Saukko E, Ovaska T, Sirviö K, Honkanen M, et al. Nonvolatile ultrafine particles observed to form trimodal size distributions in non-road diesel engine exhaust. Aerosol Science and Technology 2020;54:1345–58. https://doi.org/10.1080/02786826.2020.1783432.

[48] Michelsen HA, Colket MB, Bengtsson PE, D'Anna A, Desgroux P, Haynes BS, et al. A review of terminology used to describe soot formation and evolution under combustion

and pyrolytic conditions. ACS Nano 2020;14:12470–90. https://doi.org/10.1021/acsnano.0c06226.

[49] Transport & Environment. Euro VI trucks still don' t meet emission limits on the road 2021:1–32.

[50] Mayer A, Czerwinski J, Kasper M, Ulrich A, Mooney JJ. Metal oxide particle emissions from diesel and petrol engines. SAE Technical Papers 2012. https://doi.org/10.4271/2012-01-0841.

[51] Storey J, Curran S, Dempsey A, Lewis S, Walker NR, Reitz R, et al. The Contribution of Lubricant to the Formation of Particulate Matter with Reactivity Controlled Compression Ignition in Light-Duty Diesel Engines. Emission Control Science and Technology 2015;1:64–79. https://doi.org/10.1007/s40825-014-0007-2.

[52] Ouf F-X, Bourrous S, Fauvel S, Kort A, Lintis L, Nuvoli J, et al. True density of combustion emitted particles: A comparison of results highlighting the influence of the organic contents. Journal of Aerosol Science 2019;134:1–13. https://doi.org/10.1016/j.jaerosci.2019.04.007.

[53] Momenimovahed A, Olfert JS. Effective Density and Volatility of Particles Emitted from Gasoline Direct Injection Vehicles and Implications for Particle Mass Measurement. Aerosol Science and Technology 2015;49:1051–62. https://doi.org/10.1080/02786826.2015.1094181.

[54] Momenimovahed A, Liu F, Thomson KA, Smallwood GJ, Guo H. Effect of fuel composition on properties of particles emitted from a diesel–natural gas dual fuel engine. International Journal of Engine Research 2021;22:77–87. https://doi.org/10.1177/1468087419846018.

[55] Zelenyuk A, Reitz P, Stewart M, Imre D, Loeper P, Adams C, et al. Detailed characterization of particulates emitted by pre-commercial single-cylinder gasoline compression ignition engine. Combustion and Flame 2014;161:2151–64. https://doi.org/10.1016/j.combustflame.2014.01.011.

[56] Ketterer JE, Cheng WK. A study of soot formation in a rapid compression machine at conditions representative of cold-fast-idle in spark ignition engines. International Journal of Engine Research 2019;20:670–7. https://doi.org/10.1177/1468087418777663.

[57] Macián V, Monsalve-Serrano J, Villalta D, Fogué-Robles Á. Extending the potential of the dual-mode dual-fuel combustion towards the prospective EURO VII emissions limits using gasoline and OMEx. Energy Conversion and Management 2021;233. https://doi.org/10.1016/j.enconman.2021.113927.

[58] Zhang T, Eismark J, Munch K, Denbratt I. Effects of a wave-shaped piston bowl geometry on the performance of heavy duty Diesel engines fueled with alcohols and biodiesel blends. Renewable Energy 2020;148:512–22. https://doi.org/10.1016/j.renene.2019.10.057.

[59] Hallquist ÅM, Jerksjö M, Fallgren H, Westerlund J, Sjödin Å. Particle and gaseous emissions from individual diesel and CNG buses. Atmospheric Chemistry and Physics 2013;13:5337–50. https://doi.org/10.5194/acp-13-5337-2013.

[60] Khalek IA, Badshah H, Premnath V, Preece D. Particle Number and Ash Emissions from a Heavy Duty Natural Gas and Diesel w / DPF Engine. 2017 ETH-Conference on Combustion Generated Nanoparticles 2017.

[61] Dimopoulos Eggenschwiler P, Schreiber D, Schröter K. Characterization of the emission of particles larger than 10 nm in the exhaust of modern gasoline and CNG light duty vehicles. Fuel 2021;291. https://doi.org/10.1016/j.fuel.2020.120074.

[62] Prikhodko VY, Curran SJ, Barone TL, Lewis SA, Storey JM, Cho K, et al. Emission characteristics of a diesel engine operating with in-cylinder gasoline and diesel fuel blending. SAE International Journal of Fuels and Lubricants 2010;3:946–55. https://doi.org/10.4271/2010-01-2266.

[63] Zhang Y, Ghandhi J, Rothamer D. Comparisons of particle size distribution from conventional and advanced compression ignition combustion strategies. International Journal of Engine Research 2018;19:699–717. https://doi.org/10.1177/1468087417721089.

[64] Bock N, Jeon J, Kittelson D, Northrop WF. Solid Particle Number and Mass Emissions from Lean and Stoichiometric Gasoline Direct Injection Engine Operation. SAE Technical Papers 2018;2018-April:1–10. https://doi.org/10.4271/2018-01-0359.

[65] Awad OI, Ma X, Kamil M, Ali OM, Zhang Z, Shuai S. Particulate emissions from gasoline direct injection engines: A review of how current emission regulations are being met by automobile manufacturers. Science of the Total Environment 2020;718:137302. https://doi.org/10.1016/j.scitotenv.2020.137302.

[66] Liu S, Zhang H, Fan Q, Wang W, Qi Y, Wang Z. Investigation of combustion and particle number (PN) emissions in a spark induced compression ignition (SICI) engine for ethanol-gasoline blends. Fuel 2022;316:123155. https://doi.org/10.1016/j.fuel.2022.123155.

[67] Lou D, Wang T, Fang L, Tan P, Hu Z, Zhang Y, et al. Investigation of the combustion and particle emission characteristics of a GDI engine with a 50 MPa injection system. Fuel 2022;315:123079. https://doi.org/10.1016/j.fuel.2021.123079.

[68] García A, Monsalve-Serrano J, Lago Sari R, Fogué-Robles Á. Use of EGR e-pump for Dual-Mode Dual-Fuel engines in mild hybrid architectures. Energy Conversion and Management 2021;247:114701. https://doi.org/10.1016/j.enconman.2021.114701.

[69] García A, Monsalve-Serrano J, José Sanchís E, Fogué-Robles Á. Exploration of suitable injector configuration for dual-mode dual-fuel engine with diesel and OMEx as high reactivity fuels. Fuel 2020;280:118670. https://doi.org/10.1016/j.fuel.2020.118670.

[70] Wei J, Zeng Y, Pan M, Zhuang Y, Qiu L, Zhou T, et al. Morphology analysis of soot particles from a modern diesel engine fueled with different types of oxygenated fuels. Fuel 2020;267:117248. https://doi.org/10.1016/j.fuel.2020.117248.

[71] Yang B, Liu L, Jia S, Zhang F, Yao M. Experimental study on particle size distribution of gasoline compression ignition (GCI) at low-load condition. Fuel 2021;294:120502. https://doi.org/10.1016/j.fuel.2021.120502.

[72] Joshi A, Johnson T v. Gasoline Particulate Filters—a Review. Emission Control Science and Technology 2018;4:219–39. https://doi.org/10.1007/s40825-018-0101-y.

[73] Yang S, Deng C, Gao Y, He Y. Diesel particulate filter design simulation: A review. Advances in Mechanical Engineering 2016;8:1–14. https://doi.org/10.1177/1687814016637328.

[74] Nagy P, Zsoldos I. A Review on the Differences Between Particle Emission, Filtration and Regeneration of Particulate Filters of Diesel and Gasoline Engines. vol. 22. Springer Singapore; 2021. https://doi.org/10.1007/978-981-15-9529-5_14.

[75] Huang H. Aspects of Manufacturing Procedure and Effective Design of Recrystallized Silicon Carbide Diesel Particulate Filters. SAE Technical Papers 2020;2020-Janua:1–7. https://doi.org/10.4271/2020-01-5116.

[76] Benajes J, Garcia A, Monsalve-Serrano J, Sari R. Evaluating the Efficiency of a Conventional Diesel Oxidation Catalyst for Dual-Fuel RCCI Diesel-Gasoline Combustion. SAE Technical Papers, vol. 2018- Septe, 2018, p. 1–13. https://doi.org/10.4271/2018-01-1729.

[77] Poussin O, Gaillard P, Antonio García, Monsalve-Serrano J, Fogué Robles Á. Synthetic Fuels and Dual-Fuel RCCI : A Pathway Towards Carbon Neutrality in the Road Transport Sector. 11th Aachen Colloquium China Sustainable Mobility 2021.

[78] García A, Monsalve-Serrano J, Lago Sari R, Gaillard P. Assessment of a complete truck operating under dual-mode dual-fuel combustion in real life applications: Performance and emissions analysis. Applied Energy 2020;279:115729. https://doi.org/10.1016/j.apenergy.2020.115729.

[79] Lago Sari R. Dual Mode Dual Fuel Combustion: Implementation on a Real Medium Duty Engine Platform 2021.

[80] García A, Monsalve-Serrano J, Villalta D, Lago Sari R. Performance of a conventional diesel aftertreatment system used in a medium-duty multi-cylinder dual-mode dual-fuel engine. Energy Conversion and Management 2019;184:327–37. https://doi.org/10.1016/j.enconman.2019.01.069.

Notation

ATS: Aftertreatment System

BMEP: Break Mean Effective Pressure

C: Carbonous matter

CAD: Crank Angle Degree

CDC: Conventional Diesel Combustion

CI: Compression Ignition

CNG: Compressed Natural Gas

CO: Carbon Monoxide

CO2: Carbon Dioxide

DI: Direct Injection

DMDF: Dual-Mode Dual-Fuel

DOC: Diesel Oxidation Catalyst

DPF: Diesel Particulate Filter

EGR: Exhaust Gas Recirculation

FSN: Filter Smoke Number

GCI: Gasoline Compression Ignition

GDI: Gasoline Direct Injection

GF: Gasoline Fraction

GPF: Gasoline Particulate Filter

HC: Hydrocarbons

HCCI: Homogeneous Charge Compression Ignition

HRF: High Reactivity Fuel

ICE: Internal Combustion Engine

LTC: Low-Temperature Combustion

LRF: Low Reactivity Fuel

NO: Nitrogen Monoxide

NO2: Nitrogen Dioxide

NOx: Nitrogen Oxides

O2: Oxygen

OME: Polyoxymethylene Dimethyl Ethers

OMEx: Mixture of Polyoxymethylene Dimethyl Ethers

PAH: Polycyclic Aromatic Hydrocarbons

PFI: Port Fuel Injection

PM: Particulate Mass

PN: Particle Number

PPC: Partially Premixed Charge

PSD: Particle Size Distribution

RCCI: Reactivity-Controlled Compression Ignition

SI: Spark Ignition

SMD: Sauter Mean Diameter

SMPS: Scanning Mobility Particle Sizer

SOF: Soluble Organic Fraction

THC: Total Hydrocarbons

VGT: Variable Geometry Turbine

WHTC: World Harmonized Transient Cycle

WtW: Well-to-Wheel

Appendix

This Appendix is meant to compile relevant but not necessarily essential information to complement the study carried out in this manuscript. These results have already been studied in previous publications of the research group and are properly referenced in their original work, where more complete explanations and discussions can be found. Performance parameters and other pollutant emissions apart from particulate matter are included here to provide a complete overview of the exhaust condition prior to and after the DOC.

The combustion process is highly relevant to understanding the formation of particulate matter. Figure A1 shows how from low loads up to 50% load, the combustion process is dominated by a premixed combustion strategy in which the combustion rate is dominated by the kinetics of the fuel. At higher loads, the more diffusive combustion of the HRF becomes evident from the prolonged tail that appears in the heat release rate. This longer exposition to rich pockets within the spray enhances the formation and growth of particles. More details and extended discussion about the combustion process and the differences between the different combustion modes employed in the DMDF engine can be found in the works of García et al. [78] and Benajes et al. [31].

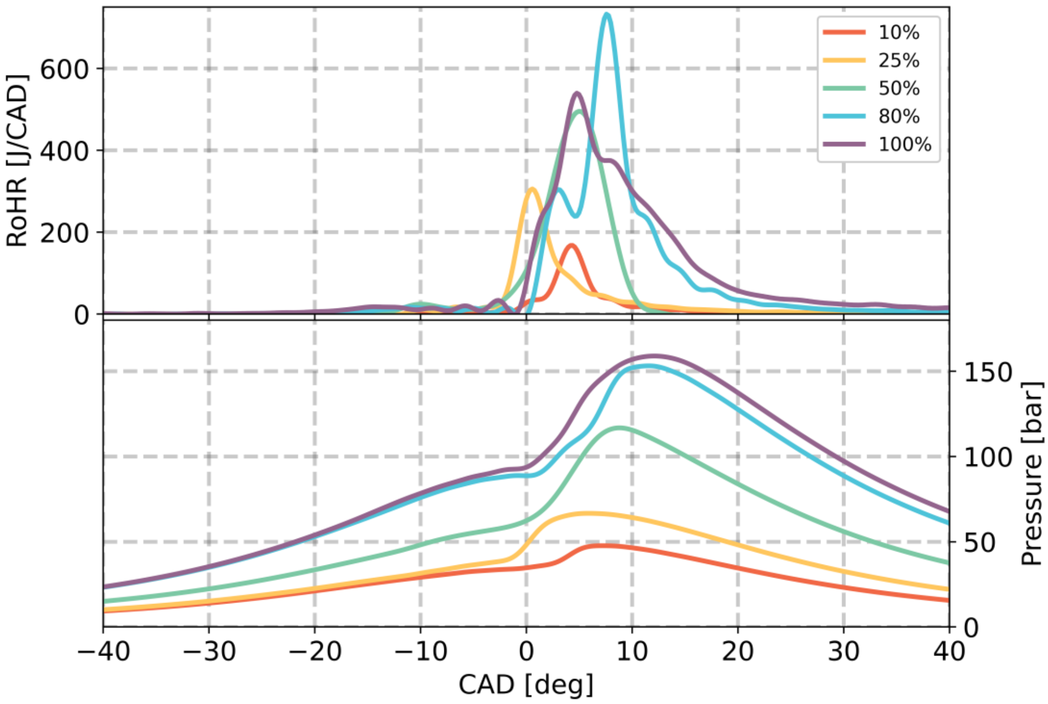

Figure A1. Heat release rate and in-cylinder pressure evolution under different engine loads at 1500 rpm.

These same works also include details abound combustion phasing and combustion duration shown in Figure A2. Up to 15 bar of BMEP, it is possible to maintain early combustion phasing to improve engine efficiency and with moderate combustion duration that permits to limit certain emissions. After that, mechanical limitations in terms of pressure gradients and peak in-cylinder pressure, as well as NOx emissions, require to delay of the combustion process to mitigate peak pressures and temperatures, but this also impacts great fuel consumption and longer combustion durations that affect soot formation.

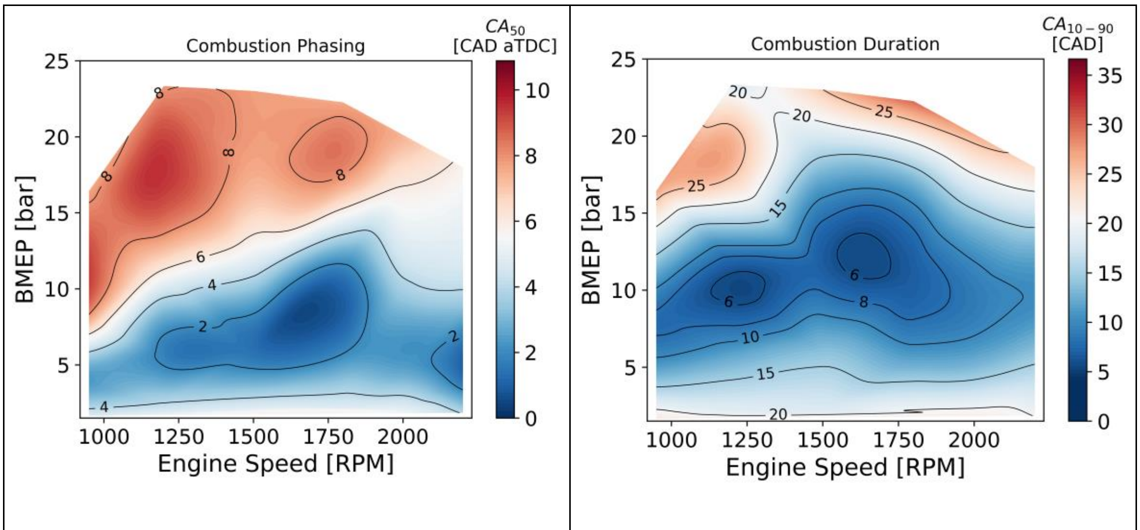

(a) (b)

Figure A2. Engine map distribution of combustion phasing (a) and combustion duration (b).

The work from Garcia et al. [78], combined with the thesis of Dr. R Sari [79], provides a thorough comparison of the DMDF technology against conventional CDC architectures under different scenarios in terms of engine efficiency and other performance parameters. The efficiency parameters included in Figure A3 show how the DMDF can maintain a global brake thermal efficiency very similar to that of the CDC along most of the engine map, achieving more than 2% of improvement in some regions. Even at full loads, it is possible to equal the engine efficiency despite the lower compression ratio. The drop in total efficiency at lower engine speeds was attributed in the work from Monsalve et al. [21] to a mismatch of the turbocharger since the original compressor and turbine were not designed to work with the increased levels of EGR that are used for the DMDF calibration.

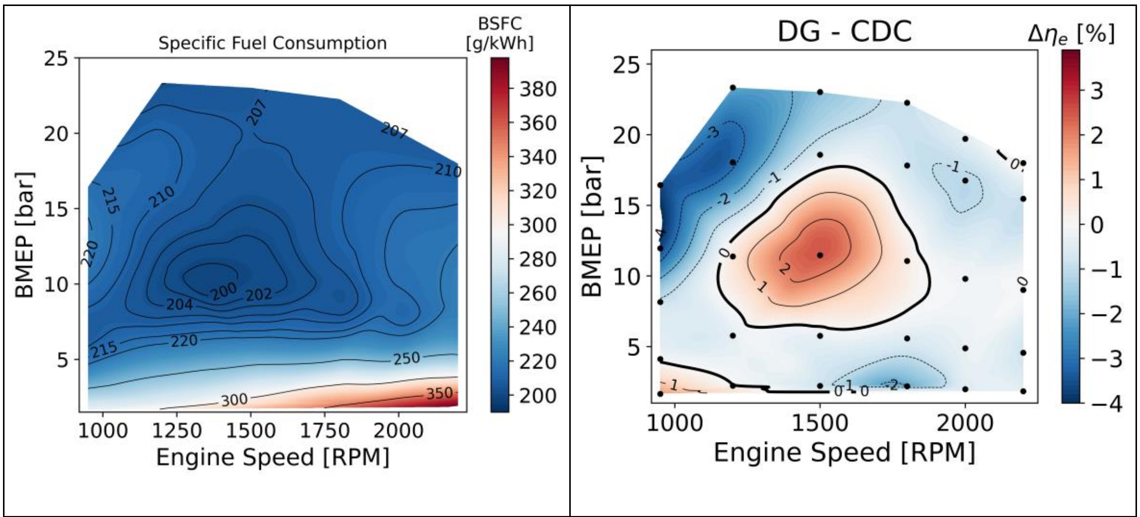

(a) (b)

Figure A3. Engine map distribution of brake specific fuel consumption (a) and comparison of brake thermal efficiency between DMDF and CDC (b).

To better understand all the reactions that are taking place through the DOC and how this can affect the particle concentrations reported in this study, it is necessary to provide a complete overview of the exact composition of the exhaust gas and how it changes after going through the catalyst. Figure A4 and Figure A5 include the concentrations of total CO and HC emitted directly by the engine, as well as how much of these species are oxidized at the catalyst by means of defining its reduction efficiency. These parameters have been previously studied in the works of Benajes et al. [31] and García et al. [80]. The graphs show a clear tendency to have greater concentrations of CO and HC emissions at lower loads as a consequence of the low temperatures and high EGR levels that dampen the completion of the combustion. Given the low exhaust temperatures, a certain region of the map does not provide sufficient energy to the DOC to light it off, but once the exhaust temperature is sufficiently high, the oxidation efficiency is high enough to ensure EURO VI levels of CO and HC emissions as reported in the previously cited works. In the case of HC emissions, the high concentrations of hydrocarbons make them prone to saturate in the exhaust line if the temperature is low enough and then be adsorbed into the particulates during their initial growth phase, increasing the number and size perceived by the measuring system.

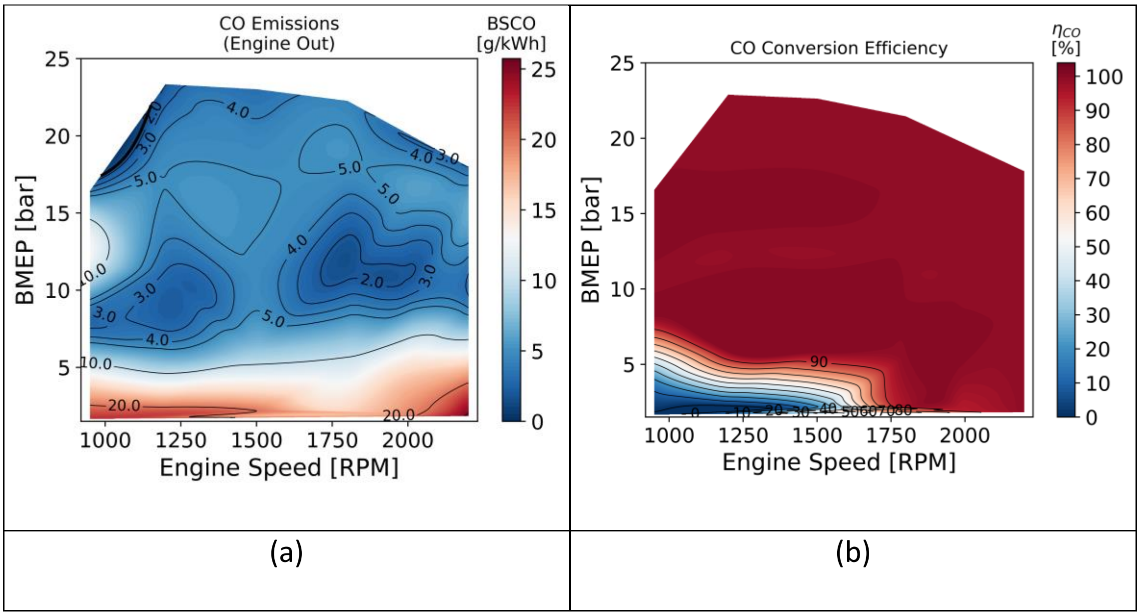

Figure A4. Evolution of engine-out CO emissions (a) and CO conversion efficiency at the DOC (b) along the DMDF engine map.

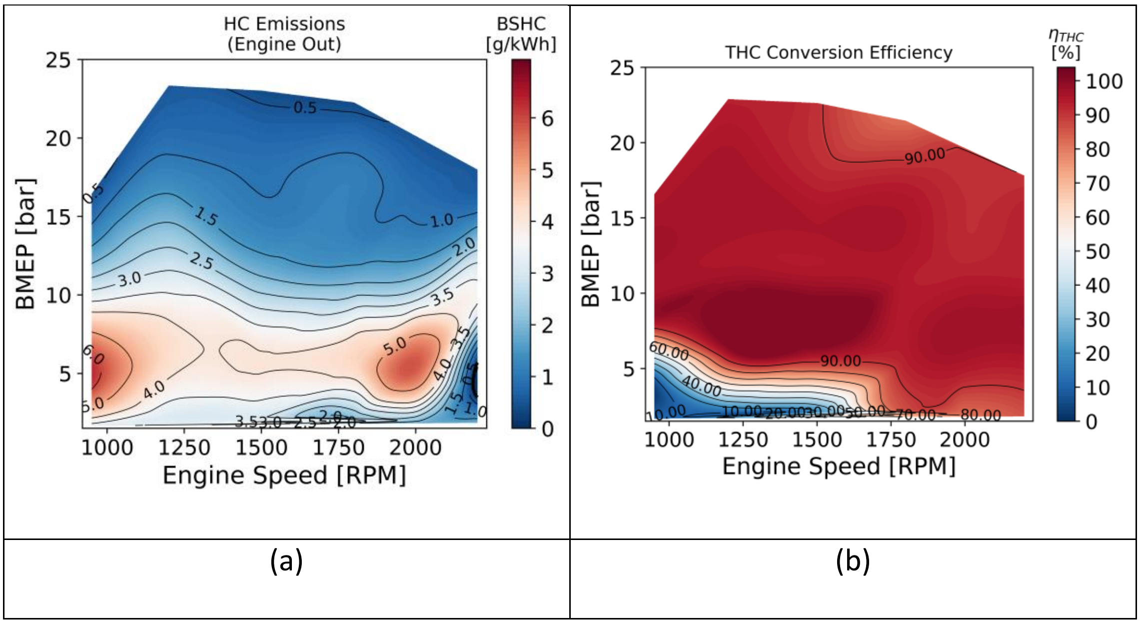

Figure A5. Evolution of engine-out HC emissions (a) and HC conversion efficiency at the DOC (b) along the DMDF engine map.

Figure A6 shows the total engine-out NOx emissions. A level below 0.4 g/kWh can be maintained for most of the engine map, extending this way to the EURO VI compliant region of the engine to ensure that global emissions during driving cycles are well within the regulation limits. This information, combined with the NO_2 fraction shown in Figure 10 and how it evolves through the DOC, provides all the information required to estimate potential passive soot regeneration in a DPF.

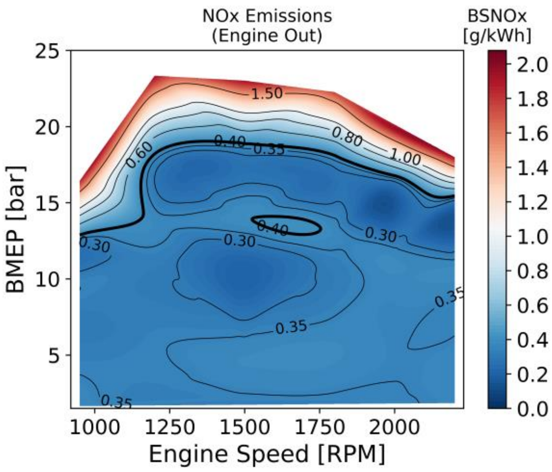

Figure A6. Evolution of engine-out NOx emissions along the DMDF engine map.

The last requirement to define the exhaust line conditions in order to understand how to address the design of a potential DPF would be the temperature delivered by the DOC. To see how the DOC is affecting the gas temperature, the two parameters provided in Figure A7 are the DOC intake temperature and the increment of temperature after the DOC. The region where the DOC is lot lighted off shows a decrease in temperature since no exothermic reaction is taking place at the DOC. Once the DOC is lighted off, the temperature increase is proportional to the sum of HC and CO concentration since the oxidation of these species is a series of exothermic reactions that heat up the exhaust line. The measurements show a total increase in temperature of up to 70 K where the CO and HC are at their peak, while this increment is lower for higher engine loads since the total emitted reactants are reduced, and total airflow is increased; therefore, the oxidation reactions do not release sufficient energy to produce a significant warp up of the gas.

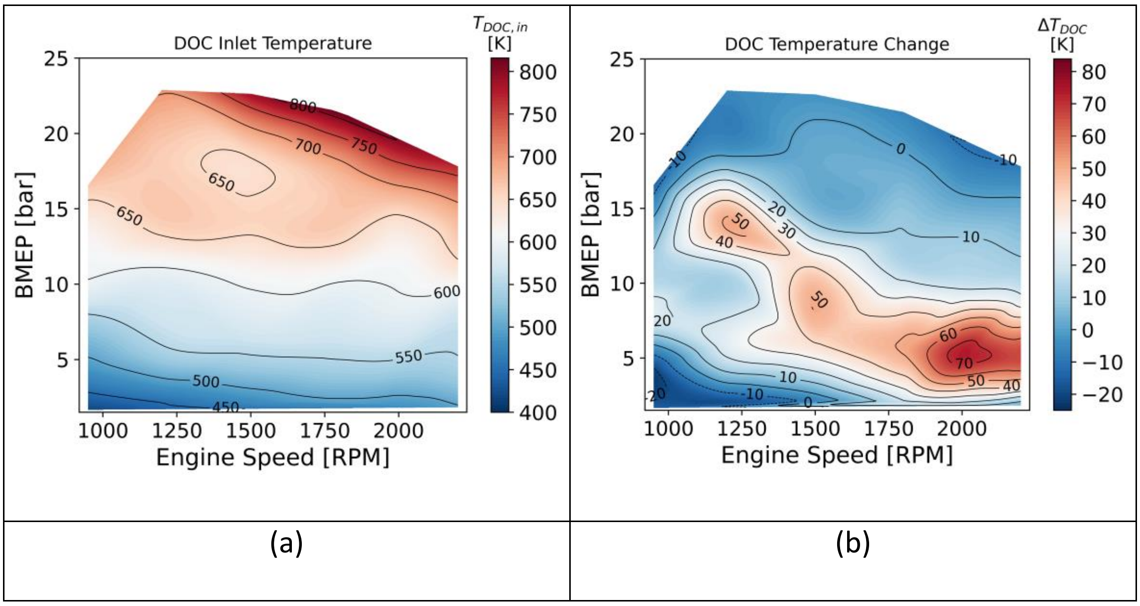

Figure A7. Evolution of DOC intake temperature (a) and temperature increase after the DOC (b) along the DMDF engine map.